~~CONFIDENTIAL~~

UNCLASSIFIED

NASA TECHNICAL MEMORANDUM

NASA TM X-900

PERSONAL COPY

NASA TM X-900

CLASSIFICATION CHANGE

To UNCLASSIFIED

By Authority of NASA CCN 211, CSTAR v8 n.24 dtd 12/31/70

Changed by _____ Date 2/13/90

SPACECRAFT AND STAGE-GEOMETRY EFFECTS ON THE HYPERSONIC CHARACTERISTICS OF A HORIZONTAL-TAKE-OFF REUSABLE BOOSTER

by Larry R. Clark and P. Kenneth Pierpont

Langley Research Center

Langley Station, Hampton, Va.

NATIONAL AERONAUTICS AND SPACE ADMINISTRATION • WASHINGTON, D. C. • NOVEMBER 1963

~~CONFIDENTIAL~~

UNCLASSIFIED

TECHNICAL MEMORANDUM X-900

SPACECRAFT AND STAGE-GEOMETRY EFFECTS ON THE HYPERSONIC CHARACTERISTICS OF A HORIZONTAL-TAKE-OFF REUSABLE BOOSTER

By Larry R. Clark and P. Kenneth Pierpont

Langley Research Center
Langley Station, Hampton, Va.

NATIONAL AERONAUTICS AND SPACE ADMINISTRATION

NATIONAL AERONAUTICS AND SPACE ADMINISTRATION

TECHNICAL MEMORANDUM X-900

SPACECRAFT AND STAGE-GEOMETRY EFFECTS ON THE HYPERSONIC CHARACTERISTICS OF A HORIZONTAL-TAKE-OFF REUSABLE BOOSTER*

By Larry R. Clark and P. Kenneth Pierpont

SUMMARY

A wind-tunnel investigation has been made at supersonic and hypersonic speeds of a preliminary horizontal-take-off reusable-booster system. The model consisted of a first-stage winged reusable booster, two interchangeable expendable second-stage rocket boosters which differed in length, and three interchangeable spacecraft as third stages. The second and third stages were combined in a tandem arrangement, and these combinations were placed parallel to the first-stage reusable booster. The tests were conducted in a 2-foot hypersonic facility at the Langley Research Center at nominal Mach numbers of 3.0, 4.5, and 6.0, angles of attack from -4° to approximately 14°, and angles of sideslip of 0° and 5°. The test Reynolds numbers per foot varied from approximately 1.0×10^6 to 2.1×10^6.

The first-stage reusable booster was longitudinally stable at all test Mach numbers for the selected moment reference center of 0.25 mean aerodynamic chord. The addition of a long second-stage booster with winged-rocket spacecraft caused a reduction in longitudinal stability, whereas the addition of a short second-stage booster with winged-rocket spacecraft had little effect. Increases in drag coefficients at zero lift of more than 100 percent resulted from the addition of some combinations of the upper stages to the first-stage reusable booster. The first-stage reusable booster had positive effective dihedral and directional stability. In general, the addition of the short second-stage booster with winged-rocket spacecraft to the reusable booster caused a decrease in effective dihedral and an increase in directional stability, whereas the addition of the long second-stage booster with winged-rocket spacecraft had the opposite effect.

The launch configurations were longitudinally stable at all test Mach numbers, and changing the positions and arrangements of the upper stages caused only moderate variations in stability at any particular Mach number. The piggyback position for the long second-stage booster with winged-rocket spacecraft provided more favorable drag characteristics than the underslung position. The launch configurations for both the short and long second-stage boosters with winged-rocket spacecraft were directionally stable, except for one case at a Mach number of 6.0, and had positive effective dihedral throughout the angle-of-attack and Mach number ranges of these tests for the assumed moment reference center.

*Title, Unclassified.

INTRODUCTION

An aerodynamic research program is being conducted at the Langley Research Center to examine various reusable-booster vehicles, including horizontal-and-vertical-take-off launch systems with first-stage winged reusable boosters. (See refs. 1, 2, and 3.) The purpose of this program is to provide data needed to assess the feasibility of reusable-booster systems.

The present paper extends the investigation of several arrangements of a preliminary concept of a horizontal-take-off reusable-booster system into the supersonic and hypersonic speed ranges. The model of the present investigation was similar, but not identical, to the model tested in reference 2 at subsonic and transonic speeds. The reusable-booster system for this investigation consisted of a winged first-stage reusable booster with parallel-mounted expendable second-stage rocket boosters with spacecraft. The spacecraft ranged from a simple ballistic nose cone to a winged rocket. Mission requirements for the reusable-booster system were established to place a maximum of approximately 30,000 pounds of spacecraft into a 300-nautical-mile-altitude orbit. The first stage was conceived to utilize turboramjet power plants with the hydrocarbon fuel carried entirely within the fuselage. However, for this investigation the model was tested without air inlets. First-stage separation was estimated to occur at a Mach number of 6.0 and an altitude of about 100,000 feet, with the upper stages sized for the specific mission. Gross take-off wing loading was assumed to be 120 lb/sq ft and the ratio of thrust to gross weight was assumed to be 0.60. The resultant landing wing loading for the reusable booster was approximately 40 lb/sq ft. The models tested were approximately 1/100 scale.

Data were obtained at nominal Mach numbers of 3.0, 4.5, and 6.0, angles of attack from -4° to approximately 14°, and angles of sideslip of 0° and 5°. The Reynolds numbers per foot varied from approximately 1.0×10^{6} to 2.1×10^{6}.

SYMBOLS

The aerodynamic characteristics of the model of the present investigation are referred to the stability axes for the longitudinal data and to the body axes for the lateral-directional data. The moment reference was chosen to be 25 percent of the mean aerodynamic chord of the first-stage wing, and was 8.24 inches forward of the model base and 0.165 inch beneath the top surface of the first-stage wing. All aerodynamic coefficients are based on the geometry of the first-stage reusable booster.

C_L lift coefficient, $\frac{\text{Lift}}{qS}$

$C_{L_{\alpha=0}}$ lift coefficient at $\alpha = 0^{\circ}$

C_D drag coefficient, $\frac{\text{Drag}}{qS}$

C_m pitching-moment coefficient, $\frac{\text{Pitching moment}}{qS\bar{c}}$

C_l rolling-moment coefficient, $\frac{\text{Rolling moment}}{qSb}$

C_n yawing-moment coefficient, $\frac{\text{Yawing moment}}{qSb}$

C_Y side-force coefficient, $\frac{\text{Side force}}{qS}$

C_{L_α} lift-curve slope, $\frac{\partial C_L}{\partial \alpha}$, per deg

$C_{m_{C_L}}$ longitudinal-stability parameter, $\frac{\partial C_m}{\partial C_L}$

$\frac{\partial C_D}{\partial C_L^2}$ drag-due-to-lift factor

C_{l_β} effective-dihedral parameter, $\frac{\Delta C_l}{\Delta \beta}$, per deg

C_{n_β} directional-stability parameter, $\frac{\Delta C_n}{\Delta \beta}$, per deg

C_{Y_β} side-force parameter, $\frac{\Delta C_Y}{\Delta \beta}$, per deg

b reference wing span, 1.0 ft

c local chord, ft

$\bar{c}$ reference mean aerodynamic chord, 0.916 ft

L/D lift-drag ratio, C_L/C_D

M free-stream Mach number

p_t stagnation pressure, atm

q free-stream dynamic pressure, lb/sq ft

R Reynolds number per foot

r local radius, in.

S	reference wing area, 0.687 sq ft
T_t	stagnation temperature, ^{o}R
x	distance measured rearward from fuselage nose, in.
α	angle of attack, deg
β	angle of sideslip, deg

Subscript:

o	conditions at zero lift

DESCRIPTION OF MODEL

The complete model or launch configuration consisted of three components, as shown in figure 1(a). The first stage (reusable booster) consisted of a semicylindrical fuselage with an ogive nose and a wing with outboard-mounted vertical fins for take-off and recovery; however, there were no air inlets. (See fig. 1(b).) The cross section of the ogive nose was semicircular, and its longitudinal shape is defined by table I. The nose was fitted to the wing by placing the reference axis along the lower surface of the wing at the plane of symmetry. The wing was an unsymmetrical wedge-slab with 2-percent maximum thickness and a leading-edge sweep of 70^{o}, and it was mounted on top of the fuselage with the camber of the wing adjacent to the fuselage. The vertical fins were symmetrical with 2-percent maximum thickness and leading-edge sweep angles of 70^{o} and 80^{o} for the upper and lower fins, respectively. Two second-stage boosters were employed which had identical circular cross sections but different lengths. They are designated short and long second-stage boosters. The third stage was represented by one of the three following types of spacecraft: a 40^{o} ballistic nose cone, a cylindrical rocket with a conical blunted nose and an interstage fairing, and a winged rocket. The winged-rocket spacecraft was identical to the cylindrical rocket spacecraft with the addition of a delta wing swept back 70^{o}. This wing section had a semicircular leading edge and a constant 0.05c thickness which resulted in a blunt trailing edge. (See fig. 1(c).)

The various combinations of the second stages and spacecraft were mounted in tandem, and these combinations were placed parallel to the first stage. The normal position of the upper stages was above the first stage in a piggyback position. In one case, however, the long second-stage booster with winged-rocket spacecraft was placed beneath the first stage in an underslung position.

The model of the present investigation was similar but not identical to the model used in reference 2. The model was a 1/2-scale version of the transonic model, except that the diameter of the first-stage reusable booster for the present investigation was enlarged from the 1/2-scale dimension of 1.26 inches to 1.65 inches in order to permit installation of the desired wind-tunnel balance. Vertical fins were also incorporated. Photographs of the model configurations are shown in figure 2, and principal model dimensions are given in table II.

APPARATUS AND TESTS

The tests were conducted in a 2-foot hypersonic facility at the Langley Research Center, described in reference 4, at nominal Mach numbers of 3.0, 4.5, and 6.0, angles of attack from -4° to approximately 14°, and angles of sideslip of 0° and 5°. The test Reynolds numbers per foot varied from approximately 1.0×10^6 to 2.1×10^6.

Static aerodynamic force and moment data were obtained by means of a six-component internally mounted strain-gage balance. All data were obtained with the model smooth (that is, no transition strips were used), and at the Reynolds numbers of these tests laminar flow is considered to exist on the model. The angles of attack and sideslip were corrected for balance and sting deflection under load. The axial force was corrected to correspond to a base pressure equal to the free-stream static pressure for the reusable-booster fuselage base, including that portion of the wing base intercepted by the fuselage. The pressure on the base of the rocket booster was not included in the calculation of the corrections. The average test conditions and typical Reynolds numbers for a flight trajectory corresponding to a dynamic pressure of 1,200 lb/sq ft are given in the following table:

M	p_t, atm	T_t, $^{\circ}R$	R, per foot	
			Test	Flight
3.0	1.0	580	2.1×10^6	2.9×10^6
4.5	1.5	770	1.0	1.9
6.0	3.5	790	1.2	1.4

It can be seen from a comparison of test and flight Reynolds numbers that significant differences exist which amount to about two orders of magnitude because the model is approximately 1/100 scale.

PRESENTATION OF RESULTS

The results of this investigation are presented in the following figures:

DISCUSSION

The basic longitudinal aerodynamic characteristics (figs. 3 to 6) have been summarized for comparison in figures 7 to 10. In addition, the basic lateral aerodynamic characteristics shown in figure 11 have been summarized in figure 12. The discussion has been arranged to show some of the effects of the spacecraft and stage geometry on the longitudinal stability and drag characteristics together with the lateral-directional characteristics of the presently conceived reusable-booster system.

Lift Characteristics

Reusable booster.- Figure 7 shows that C_{L_α} for the first-stage reusable booster decreased from about 0.025 to 0.014 as the test Mach number increased from 3 to 6. Since the first stage had a long slender body and a thin wing of only 2-percent thickness, it can be represented by a flat plate. As a matter of interest, theoretical values of C_{L_α} were calculated from supersonic flat-plate theory $\left(C_{L_\alpha} = \frac{4}{\sqrt{M^2 - 1}}\right)$ and are compared in figure 7 with the experimentally obtained values of C_{L_α} from the present tests. The agreement between the

present experimental values and the theoretical calculations, as well as the agreement with the data at $M = 4.63$ for configuration VI of reference 5, is considered good.

Launch vehicles.- Only small changes are shown in figure 7 to have occurred in the lift-curve slopes of the first stage when the upper stages were added; these changes are probably due primarily to the relative size of the first-stage wing which produced most of the lift of the launch vehicle. However, a comparison of figures 3(a), 4(a), and 5(a) indicates that the positive lift coefficients at $\alpha = 0^\circ$ for the first stage were reduced as much as 0.023 as a result of adding the short second-stage booster with the various spacecraft, whereas the addition of the long second-stage booster with spacecraft produced much smaller reductions in $C_{L_{\alpha=0}}$. These larger reductions in lift coefficient caused by adding the short second stage with spacecraft are probably due to a positive pressure field on the upper surface of the first-stage wing created by shocks from the leading edge of the spacecraft. In addition, figure 7 shows that changing the long second stage with winged-rocket spacecraft from the piggyback to the underslung position resulted in negligible decrements in $C_{L_{\alpha=0}}$ at a Mach number of 3.0, but became progressively greater with increasing Mach number. Inverting the complete model to produce a low-wing configuration reversed the signs of the increments in $C_{L_{\alpha=0}}$.

The variations in lift-curve slopes of the several launch configurations due to changing the upper-stage positions and arrangements are small $\left(\Delta C_{L_\alpha} < 0.002\right)$ throughout the test Mach number range, as shown in figure 7. In addition, the data for the two launch vehicles in figure 7 for the high-wing (model upright) and low-wing (model inverted) positions show the lift-curve slopes for the two positions to be identical in the range of low lift coefficients.

Longitudinal Stability

Reusable booster.- Figure 8 shows that the first stage was very stable longitudinally about the arbitrarily selected moment reference center of $0.25\bar{c}$. If the fact that the actual center-of-gravity location would most likely be considerably more rearward than the selected moment reference of these tests is disregarded, the static margin is shown to vary from approximately 26 to 21 percent as the test Mach number is increased from 3 to 6. Comparison of these data with those of reference 5 at $M = 4.63$ for a similar vehicle shows excellent agreement, as indicated in figure 8.

Launch vehicles.- The addition of the long second stage with winged-rocket spacecraft to the first stage caused reductions in static margin, measured over an angle-of-attack range from -2° to 2°, of about 2 to 3 percent; however, the addition of the short second stage with the same spacecraft had little effect on the stability of the first stage (fig. 8). The data of reference 2 show that the addition of the long second stage with winged-rocket spacecraft to the first stage caused decrements in the static margin of only about 2 percent or less over the subsonic and transonic speed ranges. All of the launch configurations employing the long second stage were generally less stable than those employing the short second stage, but the variations in stability with Mach number were about the

same. The maximum variation with Mach number (fig. 8) amounted to a change in static margin of about $6\frac{1}{2}$ percent over the test Mach number range.

Changing from the ballistic to the winged-rocket spacecraft produced adverse effects on longitudinal stability (up to 5 percent change in static margin), but the effects of this change in spacecraft were significant only when the spacecraft were located forward of the leading edge of the first-stage wing. (See fig. 8.) Changing the long second stage with winged-rocket spacecraft from the piggyback position to the underslung position is shown in figure 8 to produce changes of only about 2 percent in static margin throughout the test Mach number range. Figure 8 also shows that for the low-wing case (model inverted) the data were identical and are represented by a single line.

All the launch configurations are shown in figure 8 to be longitudinally stable at all test Mach numbers for the chosen moment reference center. The stability deteriorated with increasing Mach number and the rate of change with Mach number depended upon the upper-stage arrangement. Comparison of figures 4(b), 5(b), and 6(b) shows that positive values of $C_{m,o}$ of approximately the same magnitude were obtained for all configuration arrangements of the model in the upright position which corresponded to a high-wing booster configuration. However, if the model is inverted, which corresponds to a low-wing booster arrangement, a negative $C_{m,o}$ value was measured. This negative $C_{m,o}$ would be important in terms of the trim requirements for the vehicle and may reflect in the form of reductions in the L/D available for the entire booster model because of the adverse trim drag required for the low-wing configuration compared with the upright or high-wing configuration.

Drag and Lift-Drag Characteristics

Reusable booster.- The drag coefficients at zero lift for the first stage are shown in figure 9 to vary from approximately 0.0095 to 0.0055 throughout the Mach number range of these tests. A comparison of these data with those of reference 5 at a Mach number of 4.63 is also shown in figure 9. The close agreement of these data is interesting since the flow regime was laminar for the present tests and turbulent for that of the reference data. However, examination of the behavior of the laminar skin-friction drag coefficient with Reynolds number indicates that a large value would be expected at the low Reynolds number of the present tests (approximately 10^6). Furthermore, the behavior of the turbulent skin-friction drag coefficient with Reynolds number indicates that for the much larger Reynolds number of the reference tests (approximately 10^7), the value for the model of reference 5 would not be appreciably higher and would probably be within the experimental accuracy of the two tests. The skin-friction drag coefficients for the model of the present investigation amounted to about 40 percent of the total $C_{D,o}$ value. Thus, the agreement shown is probably fortuitous.

Drag due to lift for the first stage at low lift coefficients is shown in figure 10 to be approximately equal to the inverse of the lift-curve slope for all test Mach numbers. This result is in accord with the supersonic theory with no leading-edge suction, and close agreement with the data of reference 5 is shown.

The maximum values of L/D for the first stage (fig. 3(d)) varied from about 6.5 to 5.85 over the test Mach number range. The maximum value of L/D from reference 5 at M = 4.63 was about 6.2 which is comparable to 6.5 for the present tests at M = 4.50.

Launch vehicles.- In some cases, the addition of the upper stages to the first stage caused the drag coefficients at zero lift of the first stage alone to increase more than 100 percent (fig. 9). The maximum frontal area of the first stage constituted about 70 percent of the maximum frontal area of the entire launch vehicle, however. The maximum values of the lift-drag ratios for the launch vehicles, as well as for the first stage alone, occurred between angles of attack of approximately 3° and 8° and between lift coefficients of 0.06 and 0.15 (see figs. 3, 4, 5, and 6). The addition of the upper stages to the first stage reduced the maximum value of L/D at M = 3.00 from 6.25 to as low as 4.35, and corresponding reductions occurred throughout the test Mach number range. This reduction amounted to approximately 30 percent of the value for the first stage alone and is largely attributed to the drag increments of the second and third stages. From these reductions in L/D, it may be concluded that techniques for integrating the first and upper stages should be sought to minimize this penalty.

The drag coefficients at zero lift for the several launch configurations are given in figure 9. The highest value at M = 3.0 is shown to be 0.0180 for the short second stage with ballistic spacecraft, and for this configuration $C_{D,o}$ decreased to 0.0115 at M = 6.0. The variation with Mach number for all the configurations was similar. The launch vehicles incorporating the short second stage generally produced higher values of drag coefficient than those incorporating the long second stage. These higher values (which varied as much as 0.002 at M = 6.0) for the configurations with the short second stage compared with those with the long second stage are probably due to greater interference between the upper stages and the first-stage wing for the former configurations. This interference is thought to be primarily in the nature of shock waves from the leading edge and nose portion of the spacecraft impinging on the upper surface of the wing and reflecting on the interstage fairing between the second and third stages. Additional interference contributing to this high drag may arise from the shock interaction of the first-stage and spacecraft bow waves. Figure 9 shows that the afterbody fairing attached to the short second-stage booster produced very little reduction in drag in this Mach number range, but the fairing could be expected to provide significant improvement at transonic speeds. The effect of changing the spacecraft on the short or long second stage had a considerable effect on $C_{D,o}$ with the ballistic spacecraft producing the highest values. Changing the long second stage with winged-rocket spacecraft from the piggyback to the underslung position is shown in figure 9 to produce a significant increase in drag at zero lift for all test Mach numbers. This drag increase may be attributed to the shock waves produced by the winged-rocket spacecraft when in the underslung position; the shock waves increased the pressures along the fore portions of the ogive nose of the first stage. Adverse interference of this type and magnitude should be avoided; hence, an underslung arrangement for vehicles of this type would not be recommended.

Lateral-Directional Stability

Reusable booster.- The first stage is shown in figure 12 to have positive effective dihedral $(-C_{l_\beta})$ and directional stability throughout the entire test Mach number and angle-of-attack ranges of these tests. The effective dihedral increased with increases in angle of attack, but the directional stability remained approximately the same.

Launch vehicles.- Figure 12 shows that, in general, the addition of the short second stage with winged-rocket spacecraft to the first stage decreased the effective dihedral and increased the directional stability, whereas the addition of the long second stage with winged-rocket spacecraft had the opposite effect. Although the side force on the short second stage acts above the moment reference center, the shock waves of the spacecraft give rise to increases in pressure and a reduction in positive lift on the right wing of the reusable booster, resulting in positive rolling moments. For the case of the long second stage, the added side force is the most important factor affecting the change in C_{l_β} because the shocks in this case are probably not impinging on any large portion of the surface of the wing.

The launch configurations for the short and long second stage with winged-rocket spacecraft are shown in figure 12 to have positive effective dihedral and to be essentially stable directionally throughout the Mach number and angle-of-attack ranges of these tests. However, at $M = 6.0$ the directional stability for the long second stage with winged-rocket spacecraft deteriorated to small negative values in the low angle-of-attack range. In all cases, the effective dihedral was increased with increases in angle of attack largely associated with effective dihedral of swept wings, but the directional stability behaved with no consistent pattern. In view of the excessive static margin shown earlier, and since the center of gravity of an air-breathing booster installation is expected to be considerably rearward from the selected moment reference center, the directional stability would become unsatisfactory. Therefore, a new vertical fin configuration would be required.

SUMMARY OF RESULTS

A wind-tunnel investigation has been made of a preliminary design of a horizontal-take-off launch vehicle with a first-stage reusable booster. The aerodynamic characteristics of the first-stage reusable booster and the several launch configurations were determined at nominal Mach numbers of 3.0, 4.5, and 6.0, angles of attack from -4° to approximately 14°, and sideslip angles of 0° and 5°. The principal results are as follows:

1. All the configurations tested exhibited longitudinal stability, directional stability, except for one case at a Mach number of 6.0, and positive effective dihedral throughout the angle-of-attack and Mach number ranges of these tests for the selected moment reference center located at 0.25 mean aerodynamic chord.

2. In general, the addition of the long second-stage booster with winged-rocket spacecraft to the first-stage reusable booster caused longitudinal destabilizing increments, but the addition of the short second-stage booster with winged-rocket spacecraft had little effect. Large increases in drag coefficients of more than 100 percent resulted from the addition of some combinations of the upper stages to the first stage.

3. In general, the addition of the short second-stage booster with winged-rocket spacecraft to the first-stage reusable booster decreased effective dihedral but increased directional stability, whereas the addition of the long second-stage booster with winged-rocket spacecraft had the opposite effect.

4. Changing from the ballistic to the winged-rocket spacecraft had a significant effect on longitudinal stability only when the spacecraft were mounted forward of the leading edge of the first-stage wing.

5. The piggyback position for the long second-stage booster with winged-rocket spacecraft provided more favorable drag characteristics than the underslung position.

Langley Research Center,
National Aeronautics and Space Administration,
Langley Station, Hampton, Va., August 12, 1963.

REFERENCES

1. Pierpont, P. Kenneth: Transonic Stability of a Preliminary Vertical-Take-Off Launch Configuration With a Horizontal-Landing Recoverable Booster. NASA TM X-689, 1962.

2. Pierpont, P. Kenneth: Transonic Aerodynamic Characteristics of a Horizontal-Take-Off-and-Horizontal-Landing Recoverable-Booster Concept With Upper Stages Arranged in Parallel. NASA TM X-696, 1962.

3. Clark, Larry R., and Pierpont, P. Kenneth: Hypersonic Aerodynamic Characteristics of Preliminary Vertical-Take-Off Launch Configurations With a Horizontal-Landing Reusable Booster. NASA TM X-887, 1963.

4. Stokes, George M.: Description of a 2-Foot Hypersonic Facility at the Langley Research Center. NASA TN D-939, 1961.

5. Robins, A. Warner, Reed, James D., and Harris, Roy V., Jr.: Effects of Wing Section and Body Vertical Location on the Longitudinal Aerodynamic Characteristics at Mach Number 4.63 of a Configuration Having a 70° Delta Wing and a Low Volume Body. NASA TM X-552, 1961.

TABLE I.- SEMICIRCULAR FOREBODY COORDINATES

[Stations 0 to 8.242]

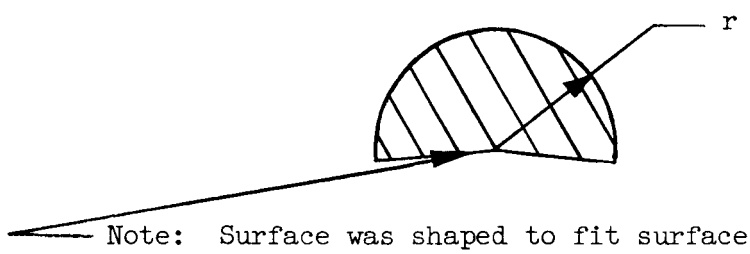

Note: Surface was shaped to fit surface of wing.

x	r
0	0
.242	.049
1.242	.232
2.242	.390
3.242	.524
4.242	.633
5.242	.717
6.242	.777
7.242	.814
8.242	.825

TABLE II.- GEOMETRIC DESIGN CHARACTERISTICS OF MODEL

Reusable booster:	
Fuselage:	
Length, in.	16.485
Diameter, in.	1.650
Forebody fineness ratio	5
Afterbody fineness ratio	5
Base area, sq in.	1.556
Wing:	
Total area, sq in.	98.910
Span, in.	12.000
Root chord, in.	16.485
Tip chord, in.	0
Thickness, percent chord (rearward of 0.40c)	2
Leading-edge sweep angle, deg	70
Leading-edge radius, in.	0.006
Mean aerodynamic chord, in.	10.990
Moment reference center, percent $\bar{c}$	25
Moment reference center, in. from base	8.243
Upper vertical tails:	
Area (exposed), sq in.	2.050
Span (exposed), in.	1.220
Root chord, in.	3.360
Tip, chord, in.	0
Thickness, percent chord (rearward of 0.40c)	2
Leading-edge sweep angle, deg	70
Lower vertical tails:	
Area (exposed), sq in.	0.991
Span (exposed), in.	0.590
Root chord, in.	3.360
Tip chord, in.	0
Thickness, percent chord (rearward of 0.40c)	2
Leading-edge sweep angle, deg	80
Short second-stage booster:	
Length, in.	6.540
Diameter, in.	1.200
Length-diameter ratio	5.450
Long second-stage booster:	
Length, in.	15.958
Diameter, in.	1.200
Length-diameter ratio	13.298
Ballistic spacecraft:	
Length, in.	1.167
Base diameter, in.	1.200
Nose cone included angle, deg	40
Nose radius, in.	0.250
Rocket spacecraft:	
Length, including interstage, in.	4.020
Interstage base diameter, in.	1.200
Interstage taper included angle, deg	40
Nose cone included angle, deg	40
Nose radius, in.	0.100
Body diameter, in.	0.500
Winged-rocket spacecraft:	
Length, including interstage, in.	4.020
Interstage base diameter, in.	1.200
Interstage taper included angle, deg	40
Nose cone included angle, deg	40
Nose radius, in.	0.100
Body diameter, in.	0.500
Total wing area, sq in.	3.845
Exposed wing area, sq in.	2.388
Span, in.	2.366
Theoretical root chord, in.	3.250
Tip chord, in.	0
Wing thickness, percent chord	10
Leading-edge sweep angle, deg	70
Leading-edge radius, percent chord	5
Afterbody fairing:	
Length, in.	3.600
Base diameter, in.	1.200

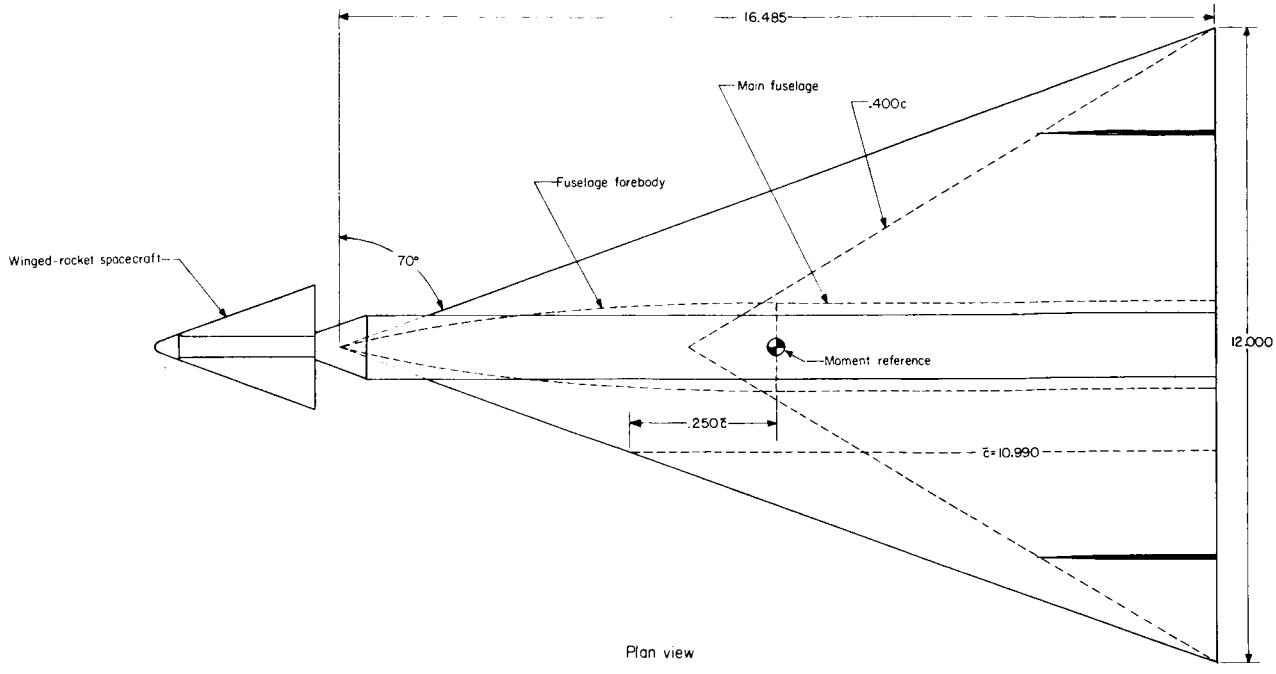

Plan view

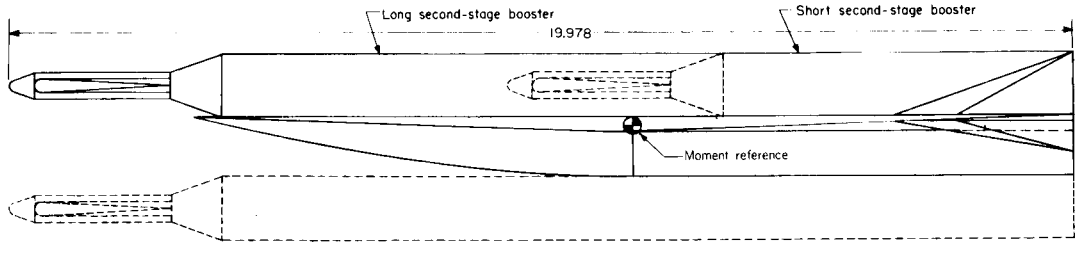

Side view

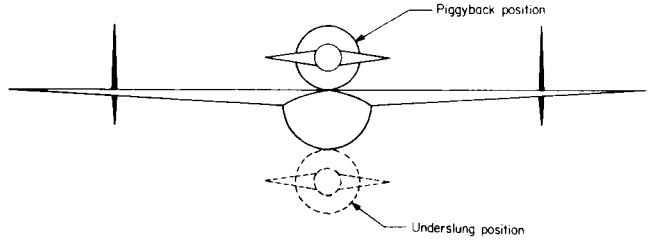

Front view

(a) General arrangement of horizontal-take-off-and-horizontal-landing reusable booster system.

Figure 1.- Arrangement and geometric details of horizontal-take-off-and-horizontal-landing launch vehicle. All linear design dimensions are in inches.

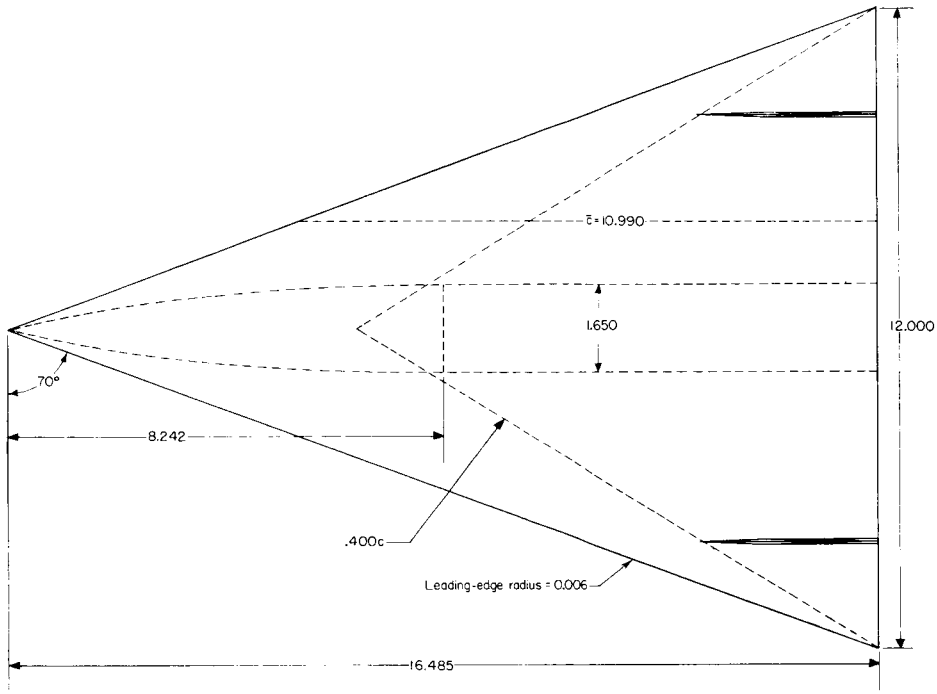

Plan view

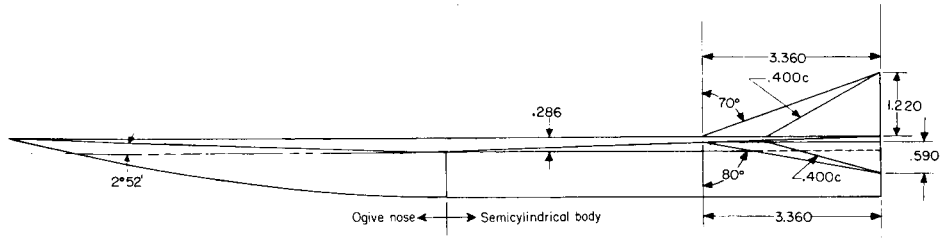

Side view

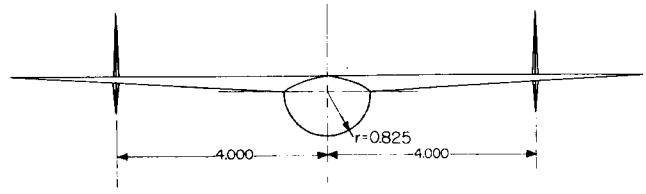

Front view

(b) First-stage reusable booster.

Figure 1.- Continued.

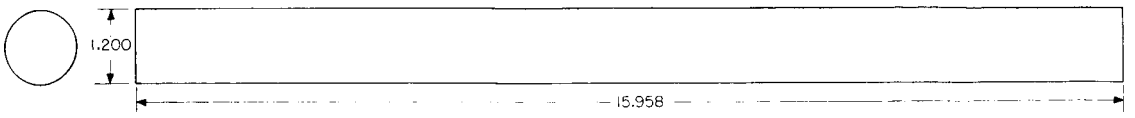

Long second-stage booster

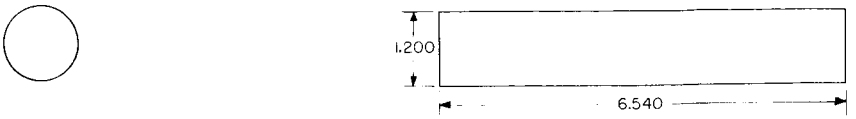

Short second-stage booster

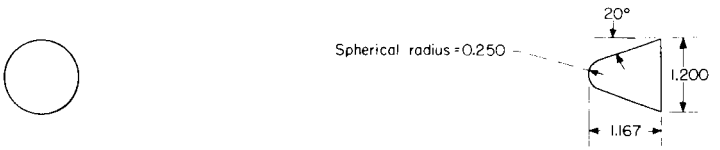

Ballistic spacecraft

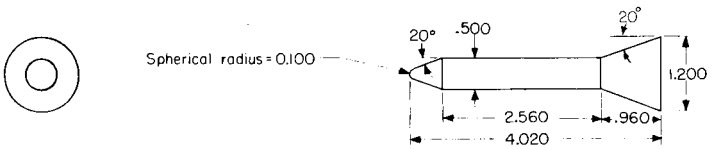

Rocket spacecraft

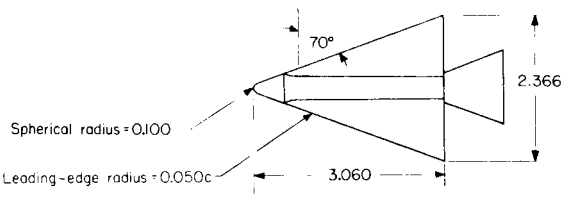

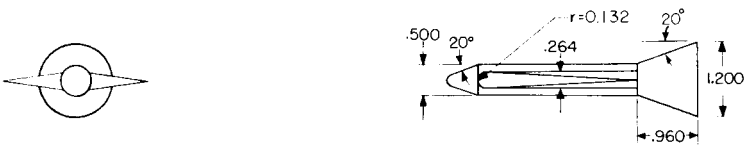

Winged-rocket spacecraft

Afterbody fairing for short second-stage booster

(c) Details of aerodynamic surface and spacecraft.

Figure 1.- Concluded.

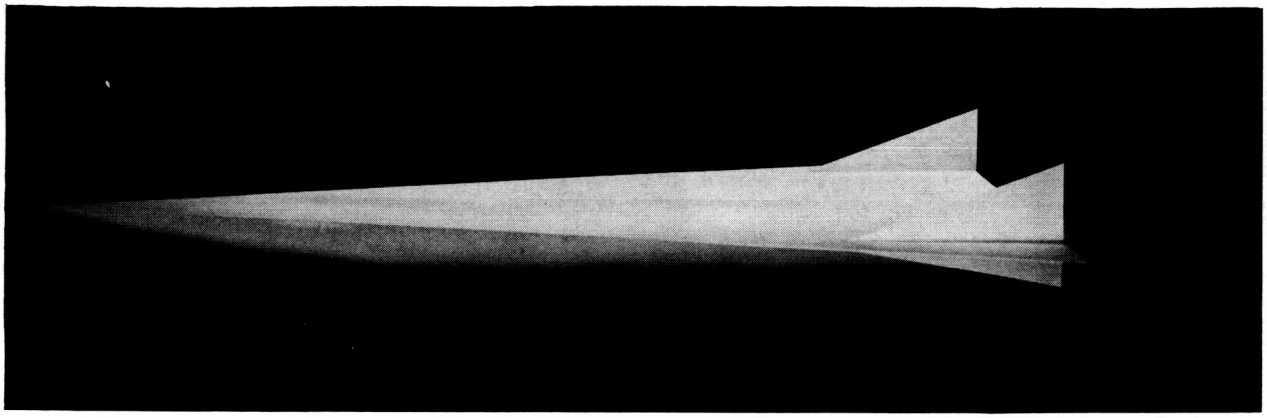

(a) First-stage reusable booster. L-62-6410

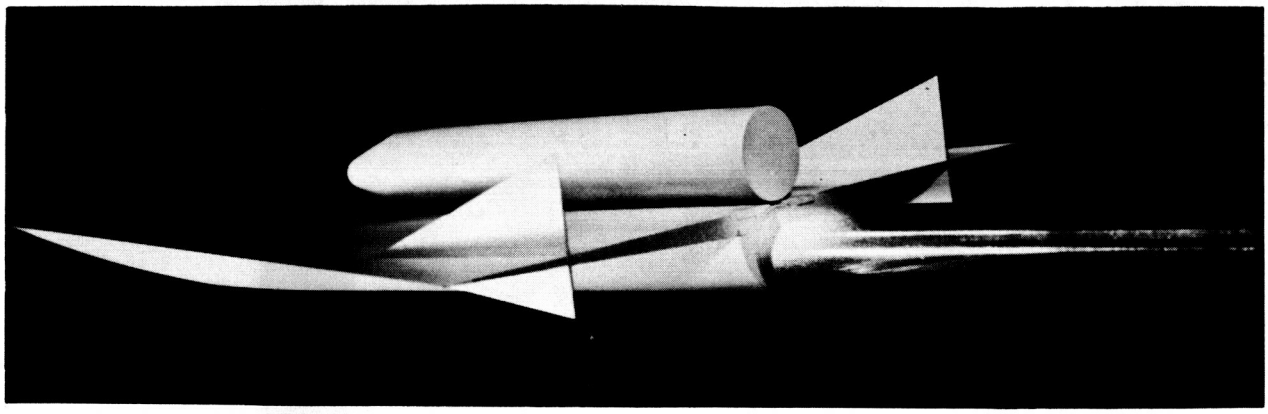

L-62-6420
(b) Short second-stage booster with ballistic spacecraft mounted above first-stage reusable booster.

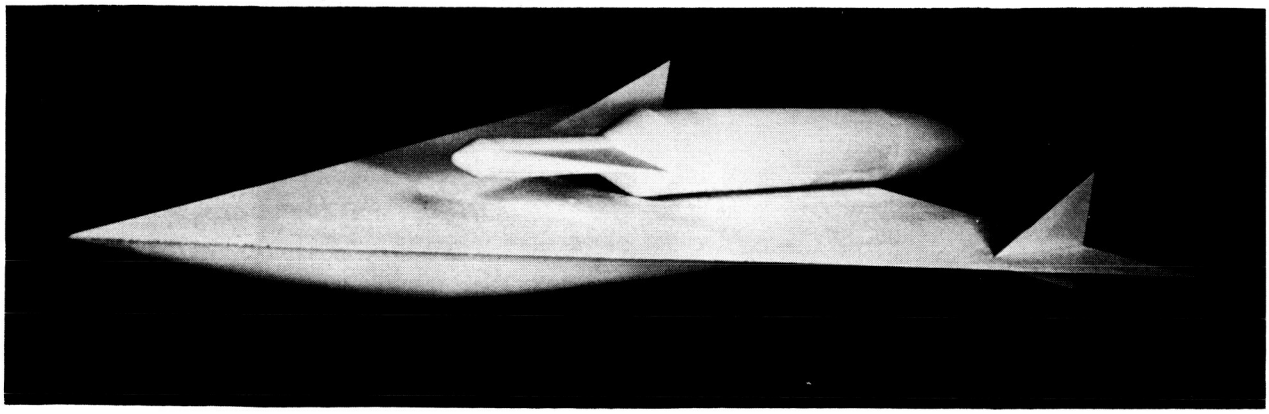

L-62-6416
(c) Short second-stage booster with winged-rocket spacecraft and afterbody fairing mounted above first-stage reusable booster.

Figure 2.- Photographs of first-stage reusable booster and launch vehicle with various upper-stage arrangements.

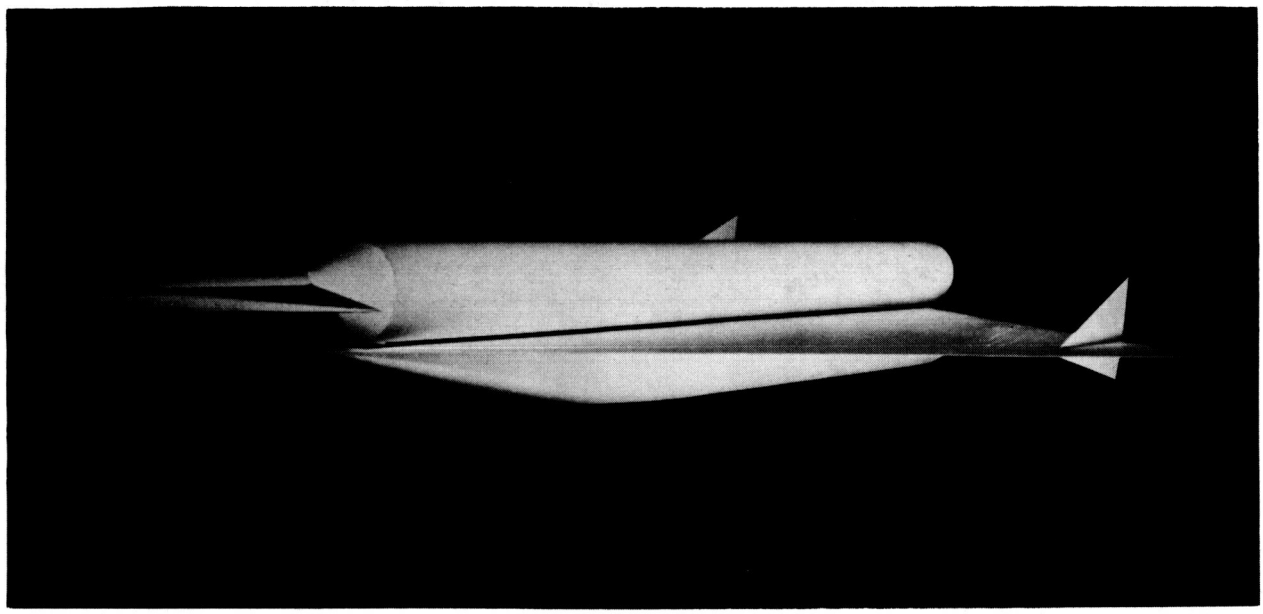

L-62-6417

(d) Long second-stage booster with winged-rocket spacecraft mounted above first-stage reusable booster.

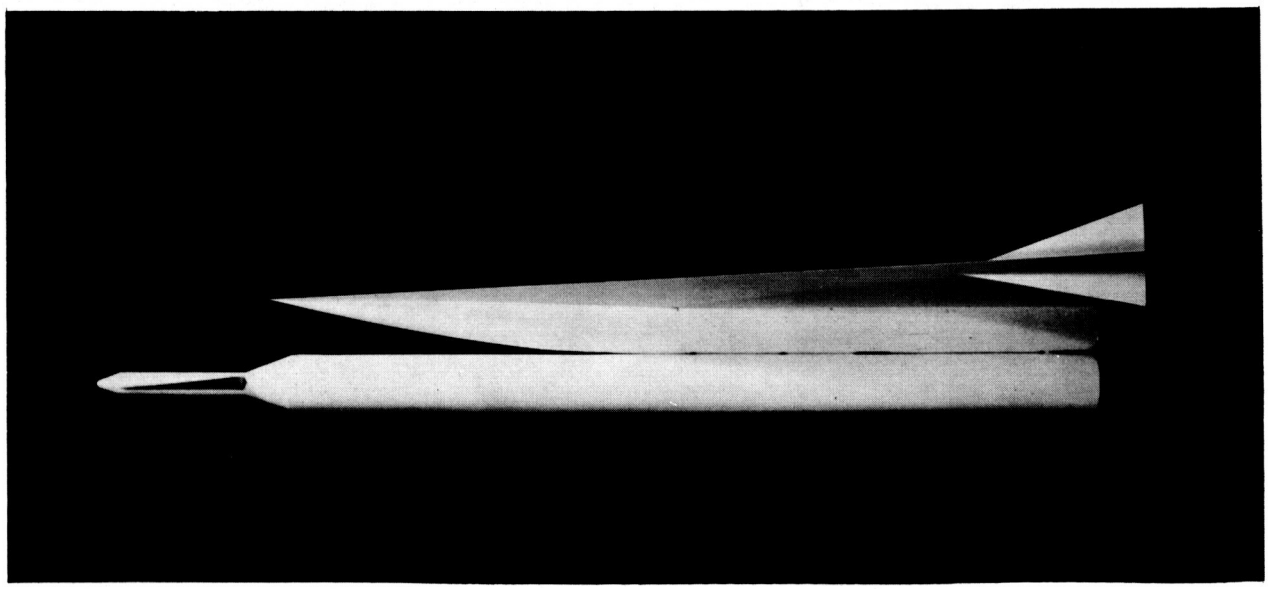

L-62-6400

(e) Long second-stage booster with winged-rocket spacecraft mounted beneath first-stage reusable booster.

Figure 2.- Concluded.

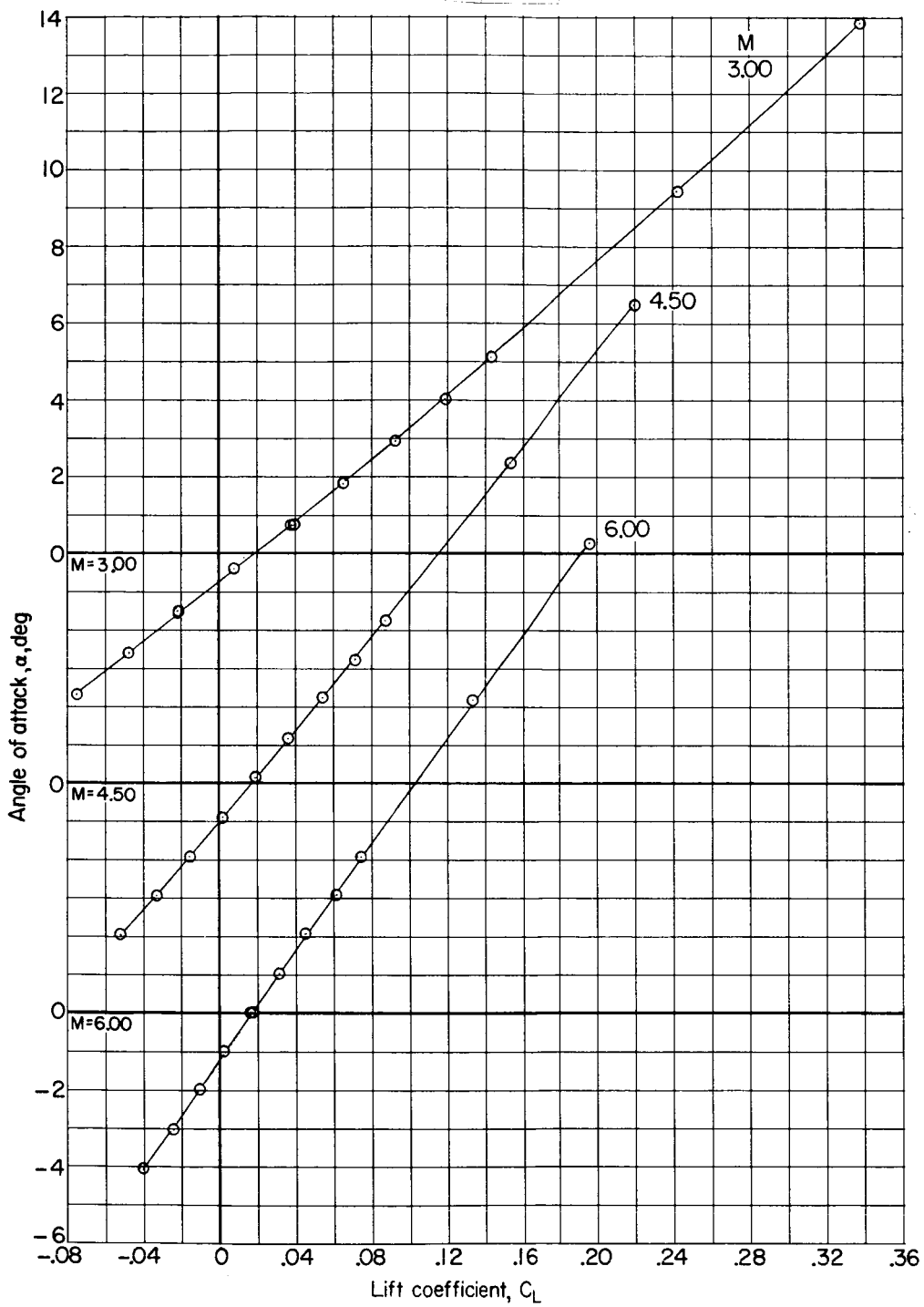

(a) Variation of lift coefficient with angle of attack.

Figure 3.- Longitudinal aerodynamic characteristics of first-stage reusable booster. $\beta = 0^{\circ}$.

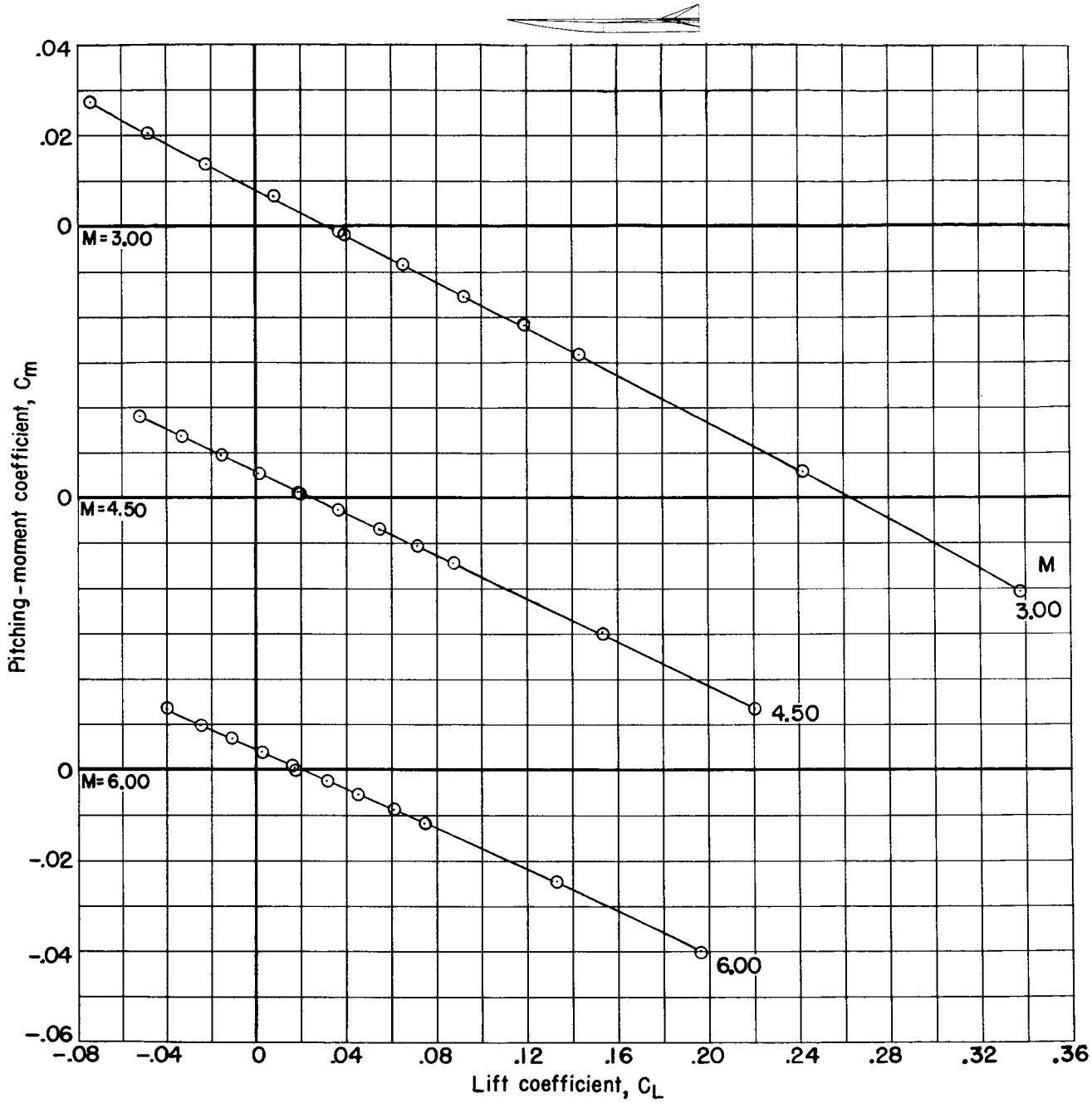

(b) Variation of pitching-moment coefficient with lift coefficient.

Figure 3.- Continued.

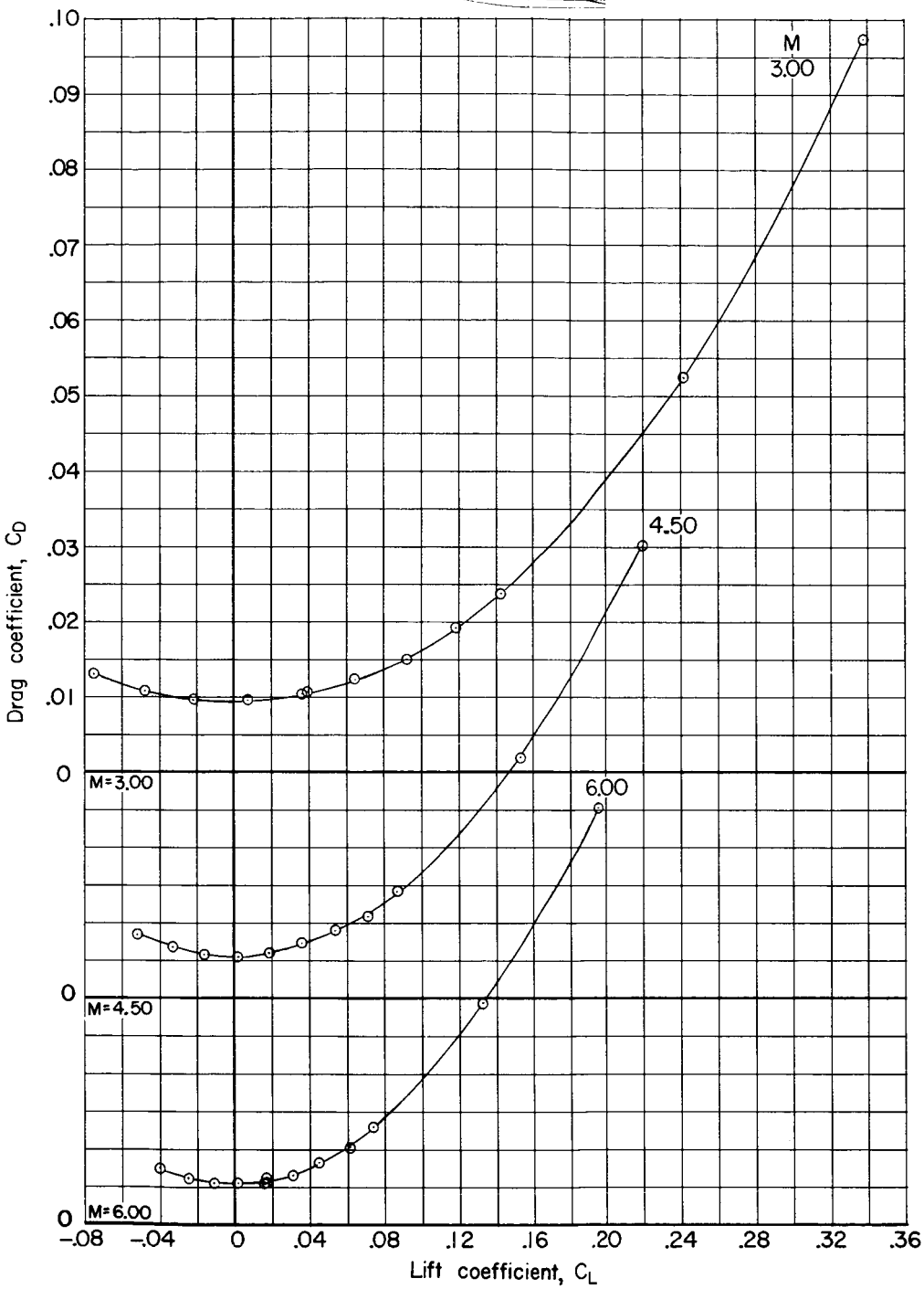

(c) Variation of drag coefficient with lift coefficient.

Figure 3.- Continued.

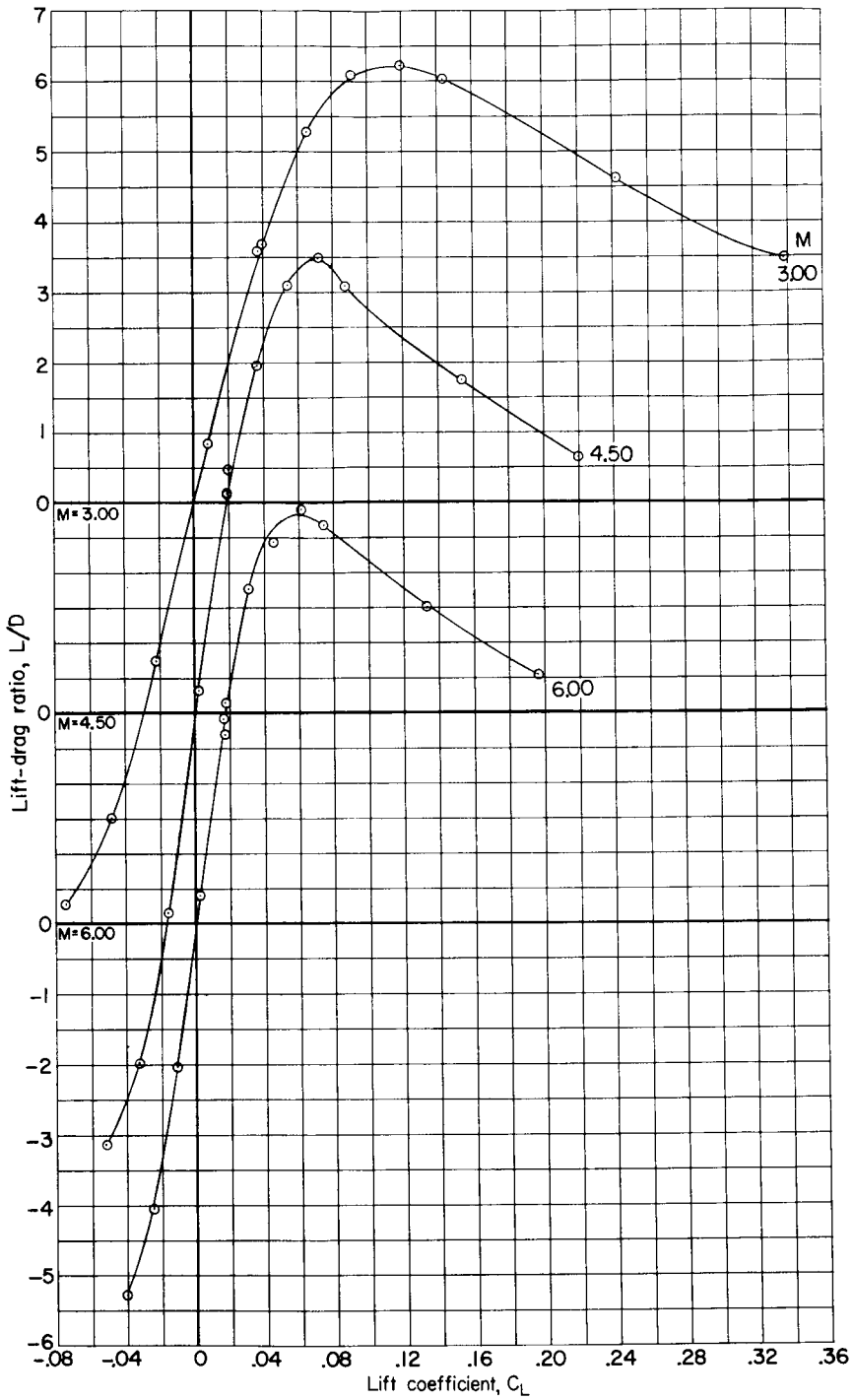

(d) Variation of lift-drag ratio with lift coefficient.

Figure 3.- Concluded.

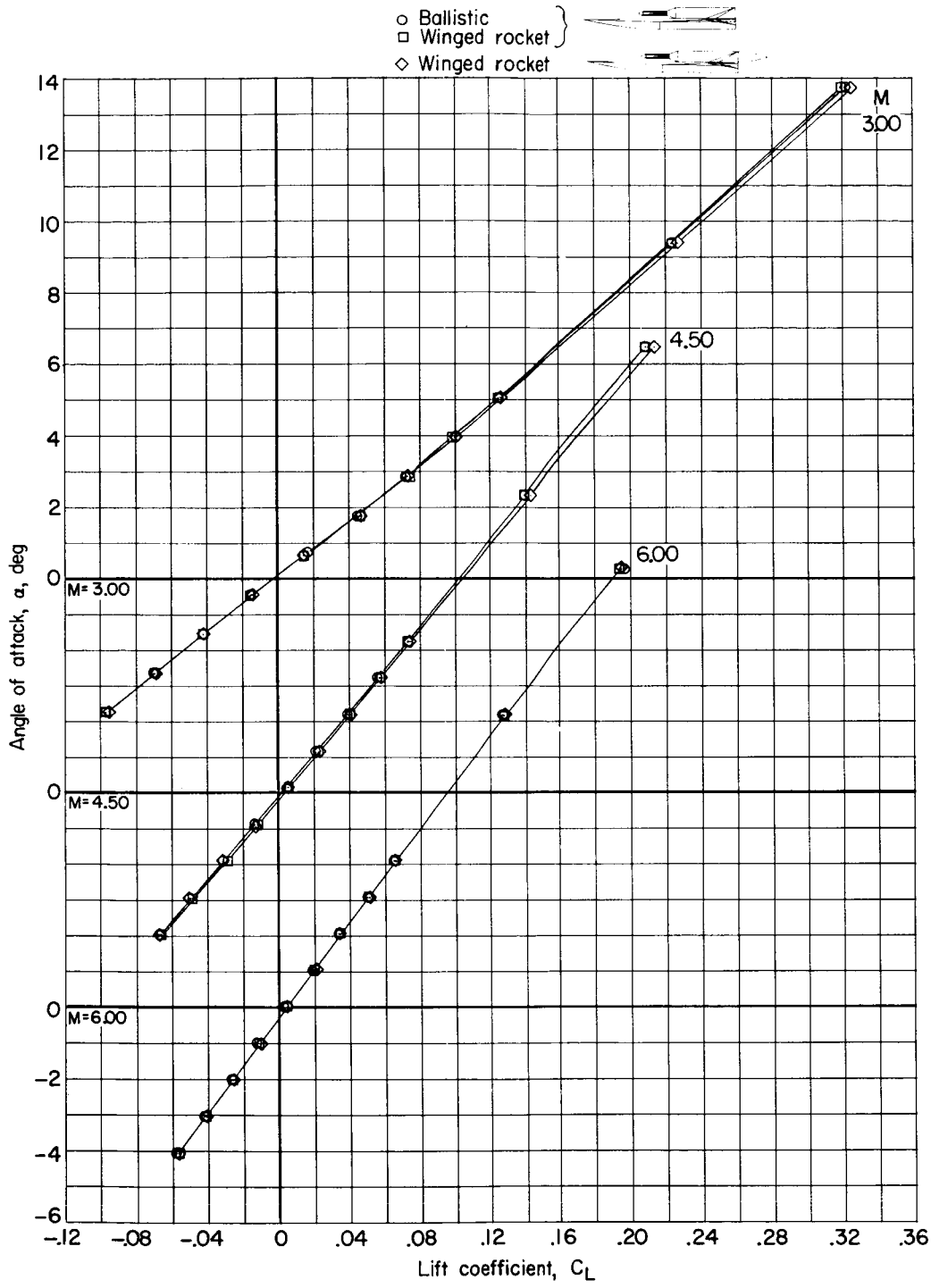

(a) Variation of lift coefficient with angle of attack.

Figure 4.- Longitudinal aerodynamic characteristics of launch configurations for short second-stage booster with ballistic and winged-rocket spacecraft including effects of afterbody fairing. $\beta = 0^{\circ}$.

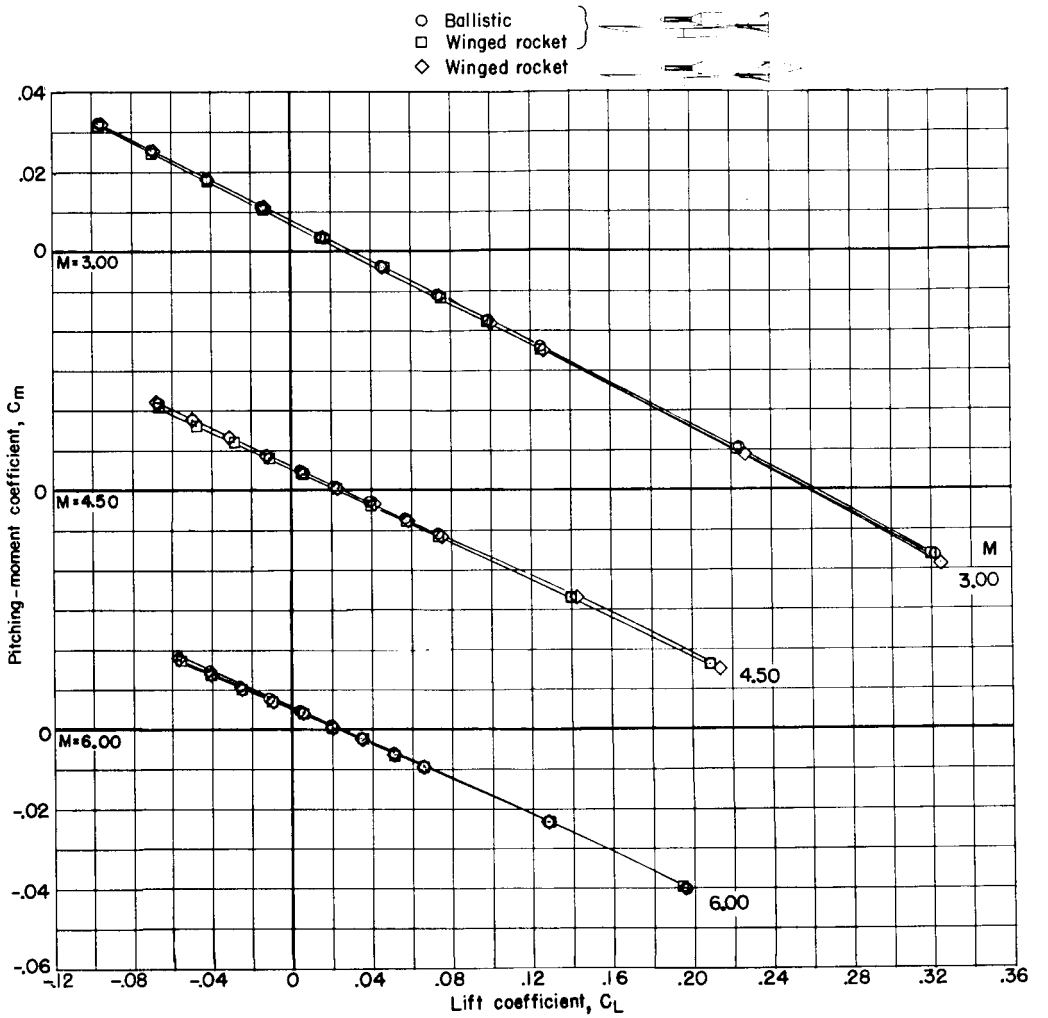

(b) Variation of pitching-moment coefficient with lift coefficient.

Figure 4.- Continued.

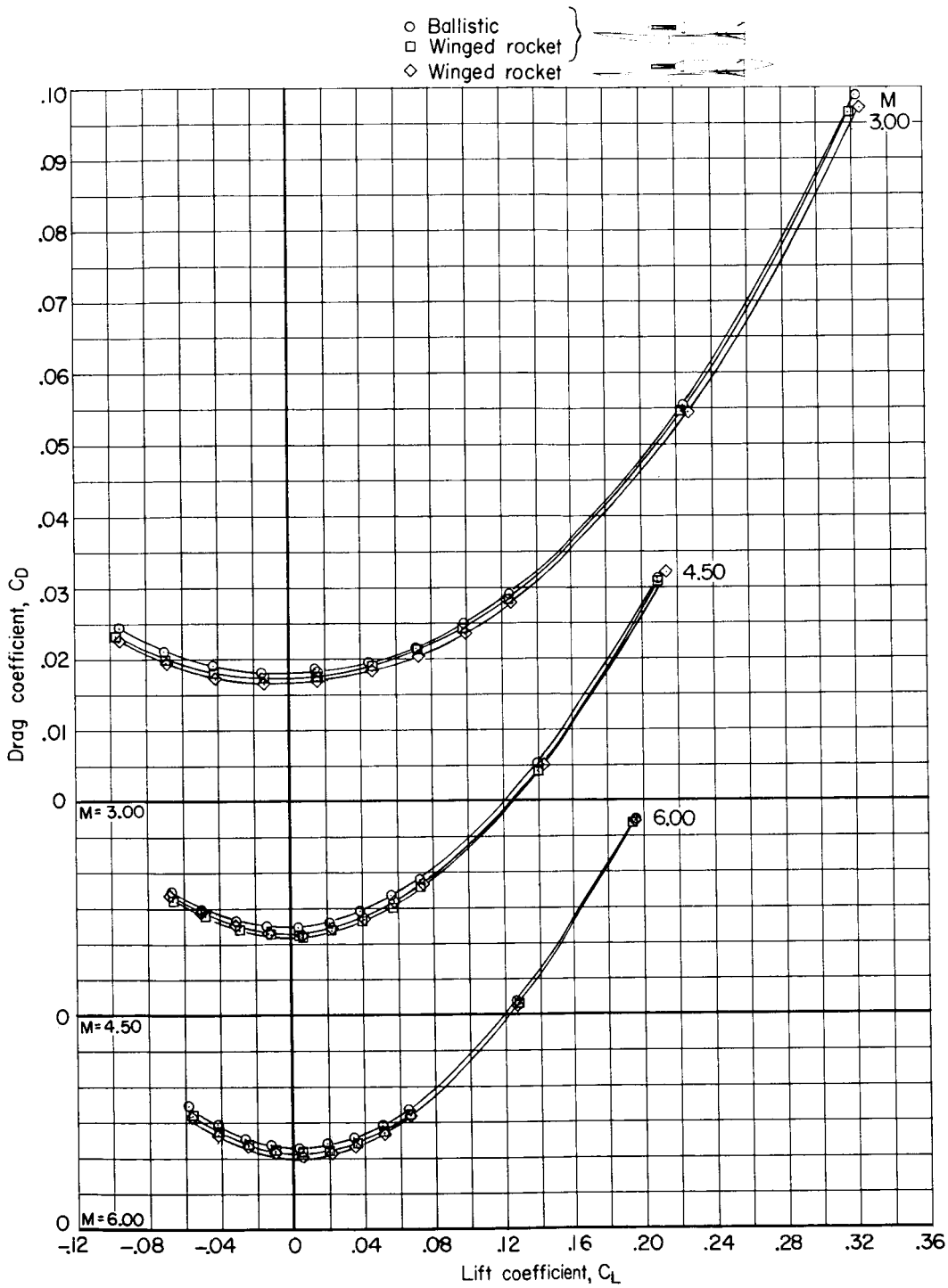

(c) Variation of drag coefficient with lift coefficient.

Figure 4.- Continued.

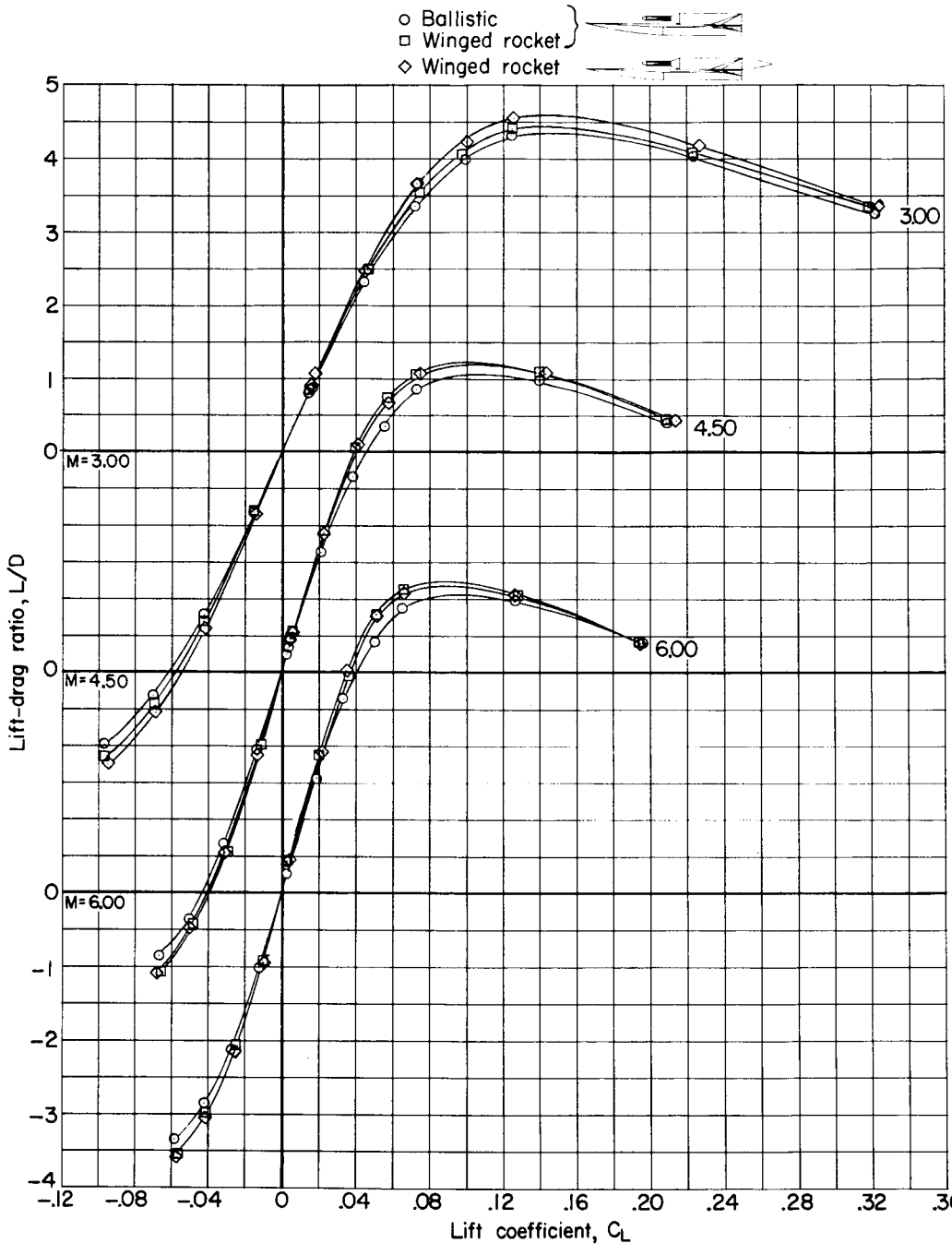

(d) Variation of lift-drag ratio with lift coefficient.

Figure 4.- Concluded.

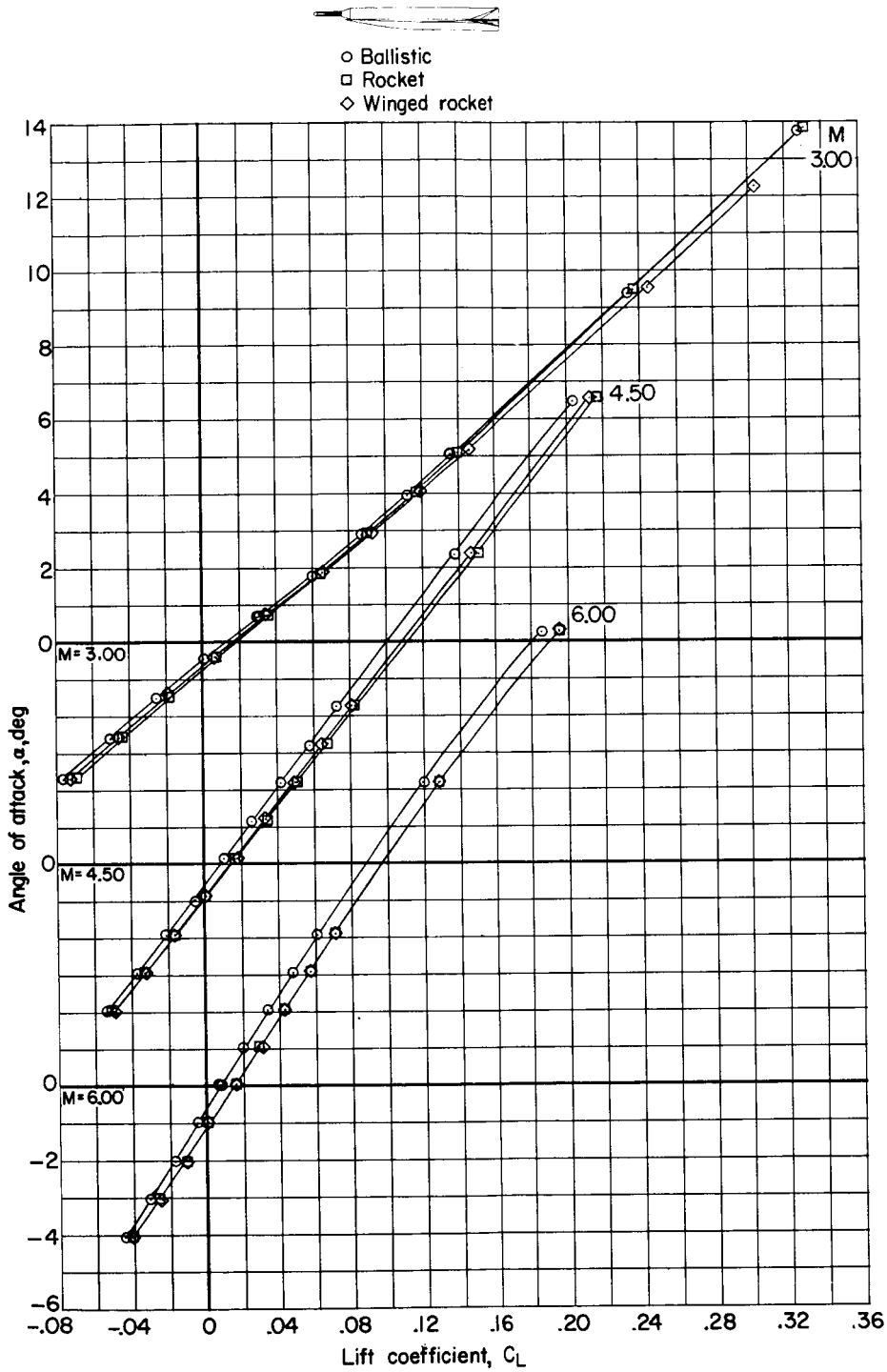

(a) Variation of lift coefficient with angle of attack.

Figure 5.- Longitudinal aerodynamic characteristics of launch configurations for long second-stage booster with ballistic, rocket, and winged-rocket spacecraft. $\beta = 0^{\circ}$.

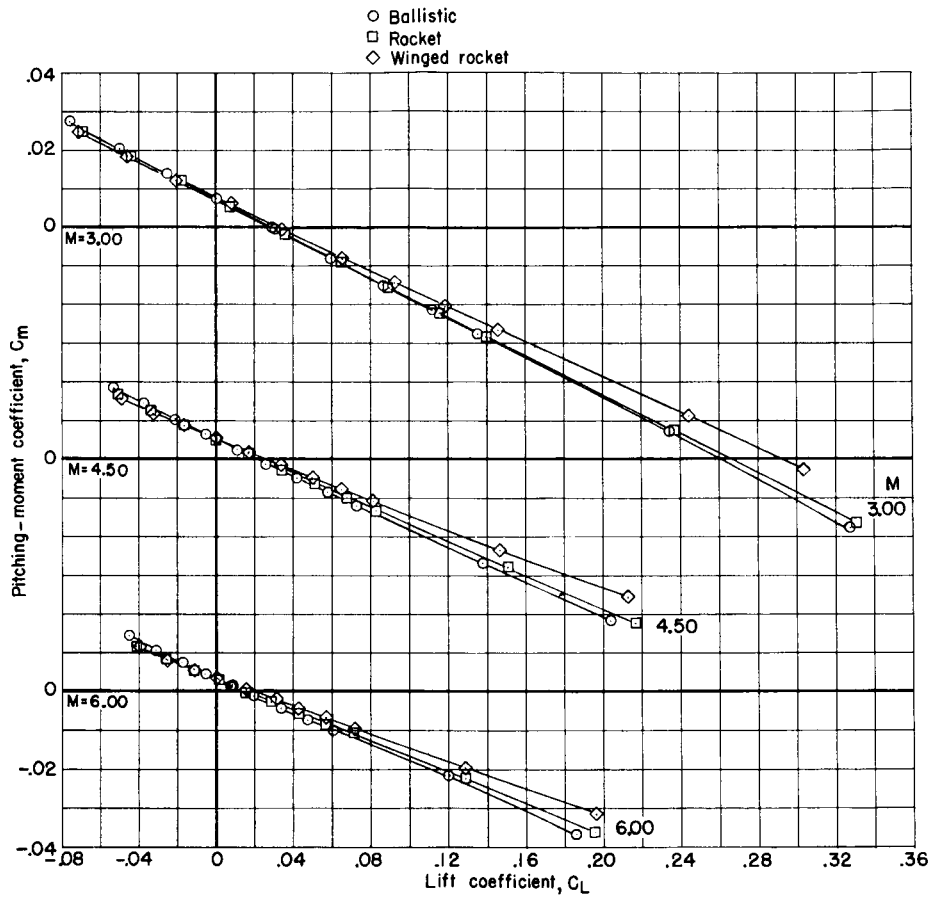

(b) Variation of pitching-moment coefficient with lift coefficient.

Figure 5.- Continued.

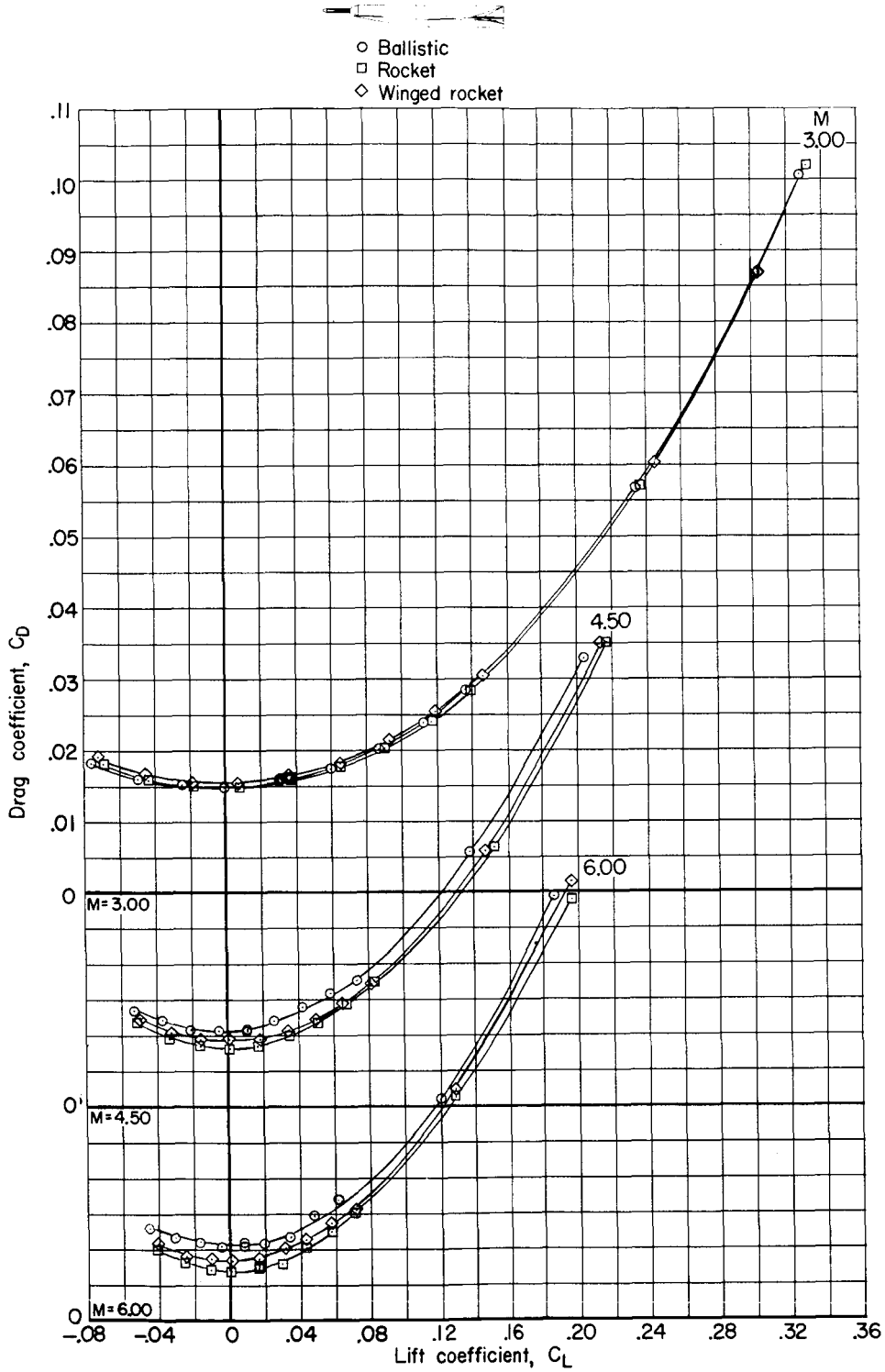

(c) Variation of drag coefficient with lift coefficient.

Figure 5.- Continued.

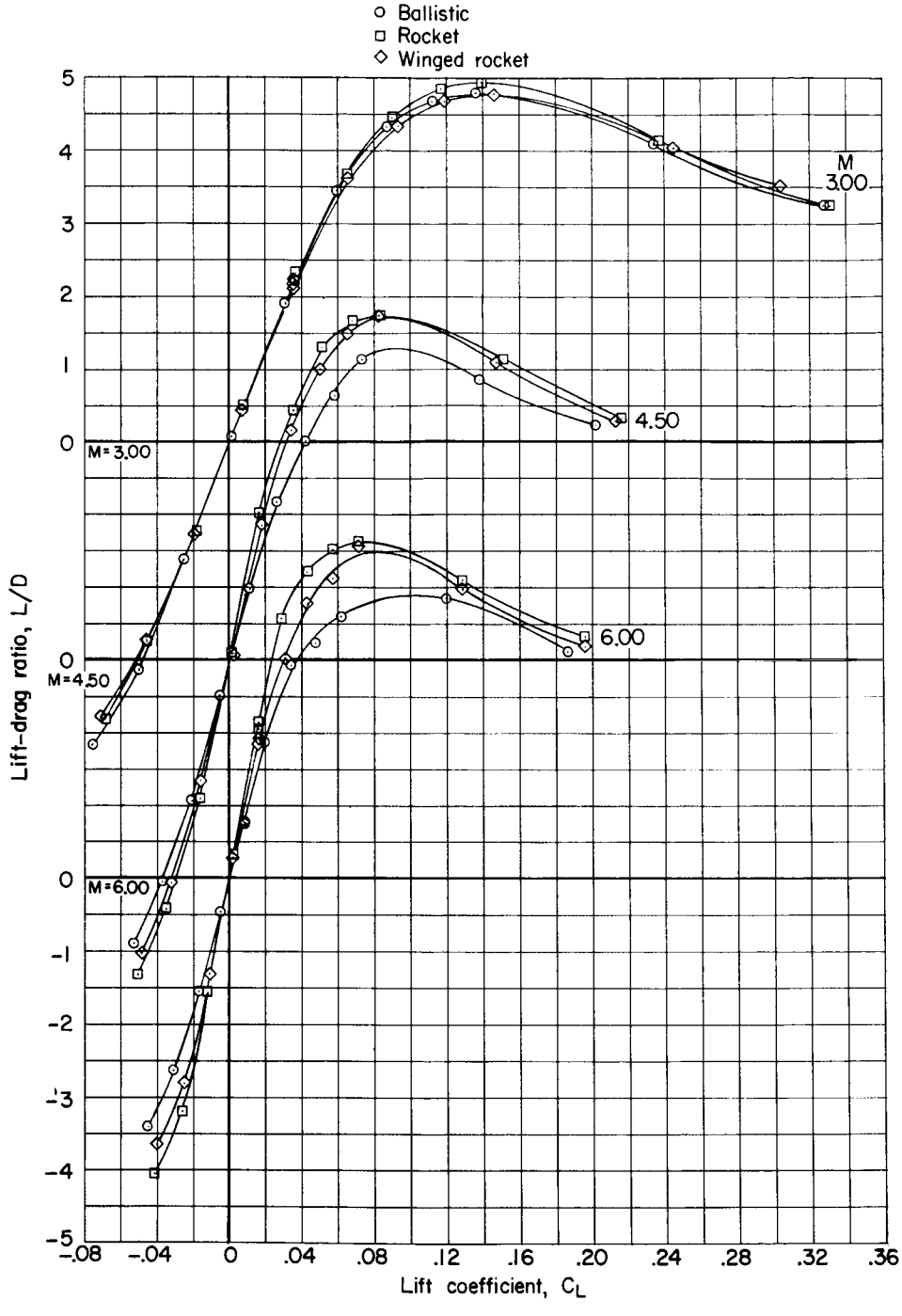

(d) Variation of lift-drag ratio with lift coefficient.

Figure 5.- Concluded.

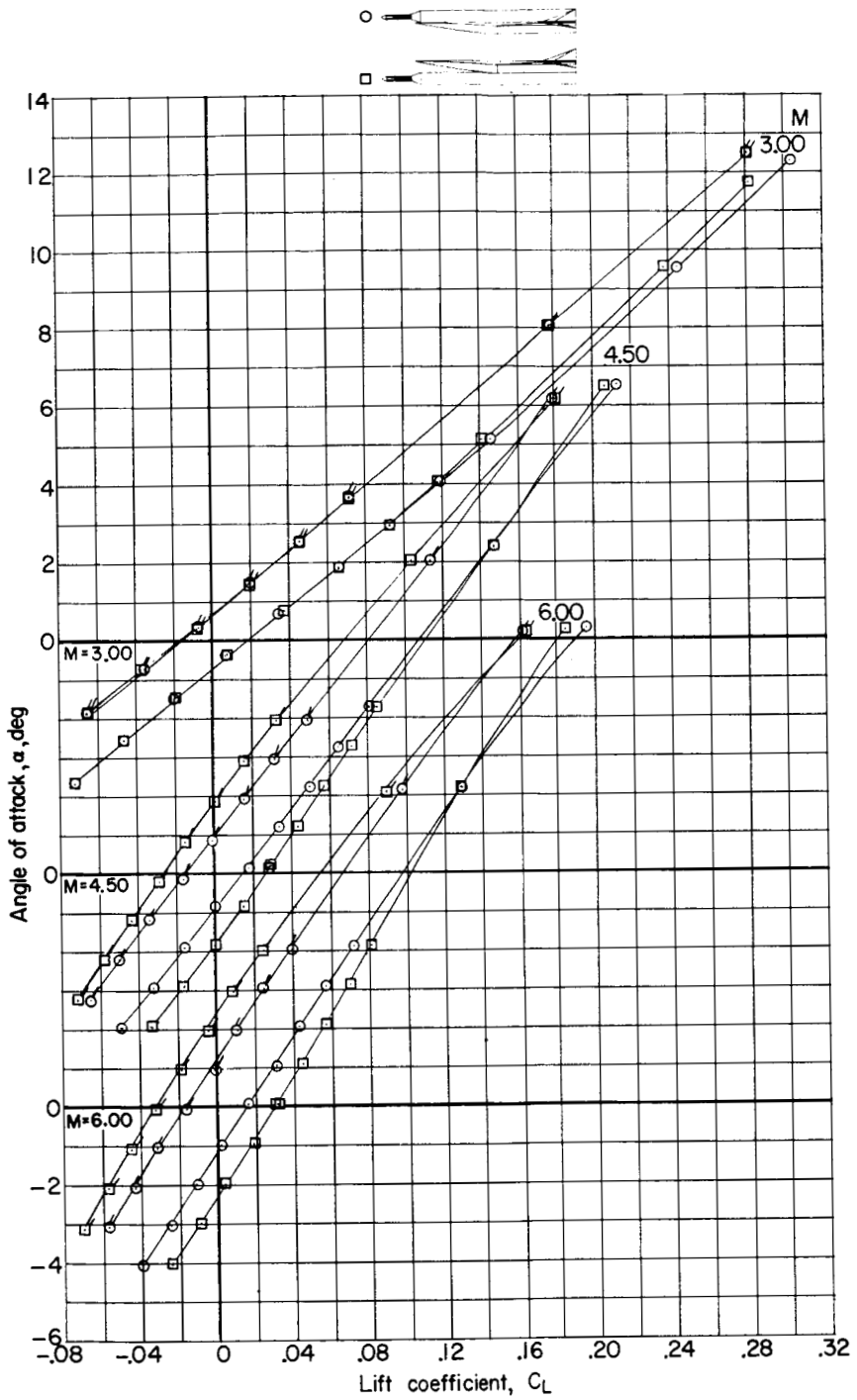

(a) Variation of lift coefficient with angle of attack.

Figure 6.- Longitudinal aerodynamic characteristics of launch configuration for long second-stage booster with winged-rocket spacecraft in piggyback and underslung positions and with models both upright and inverted. $\beta = 0^{\circ}$. (Flagged symbols refer to inverted models.)

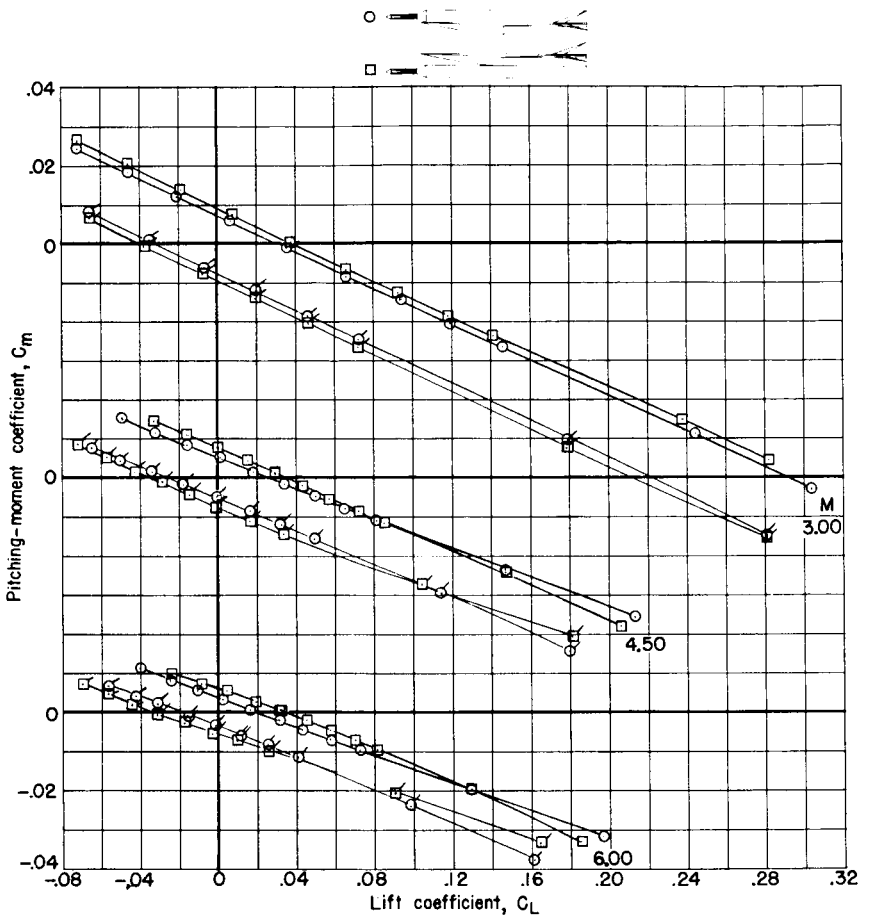

(b) Variation of pitching-moment coefficient with lift coefficient.

Figure 6.- Continued.

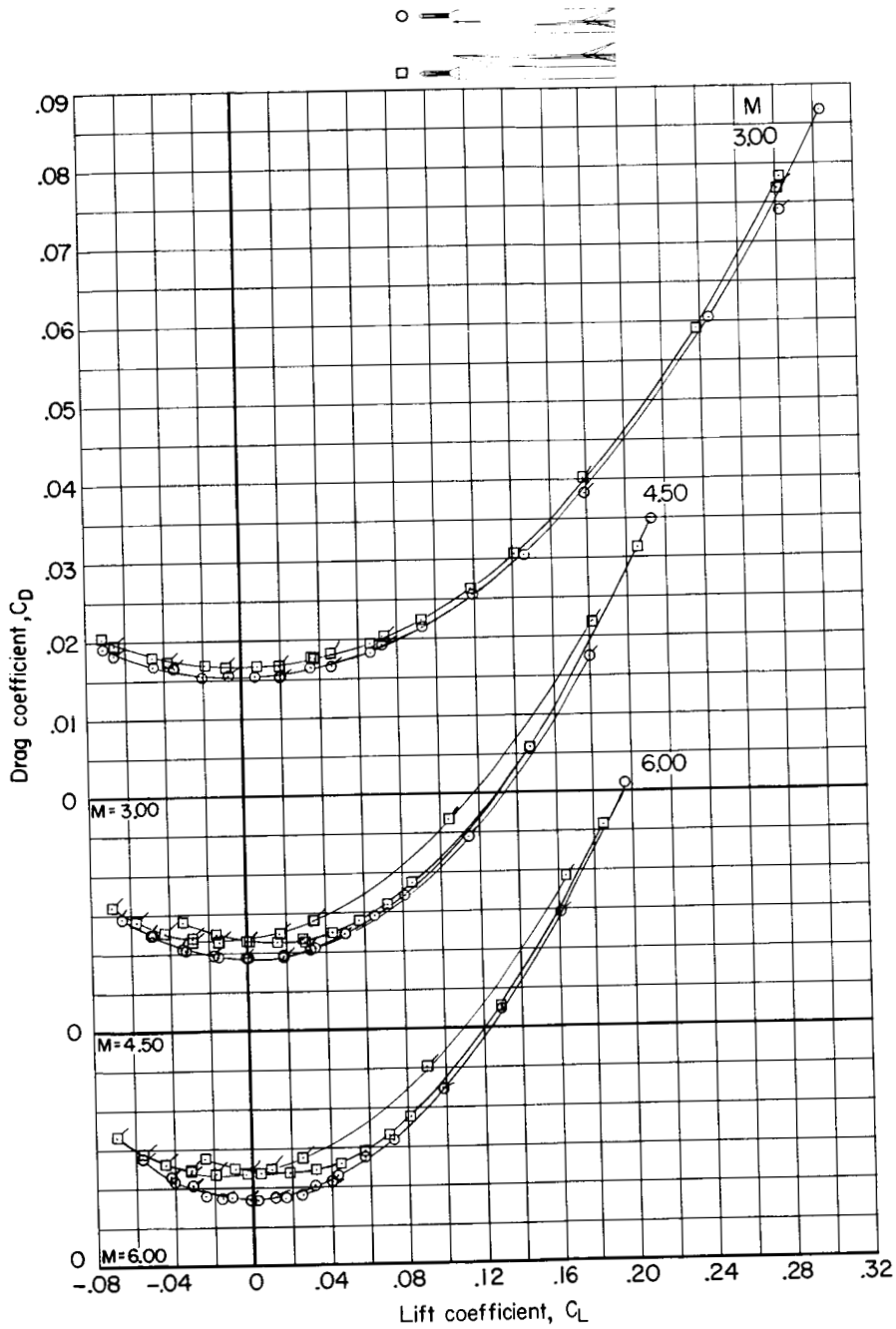

(c) Variation of drag coefficient with lift coefficient.

Figure 6.- Continued.

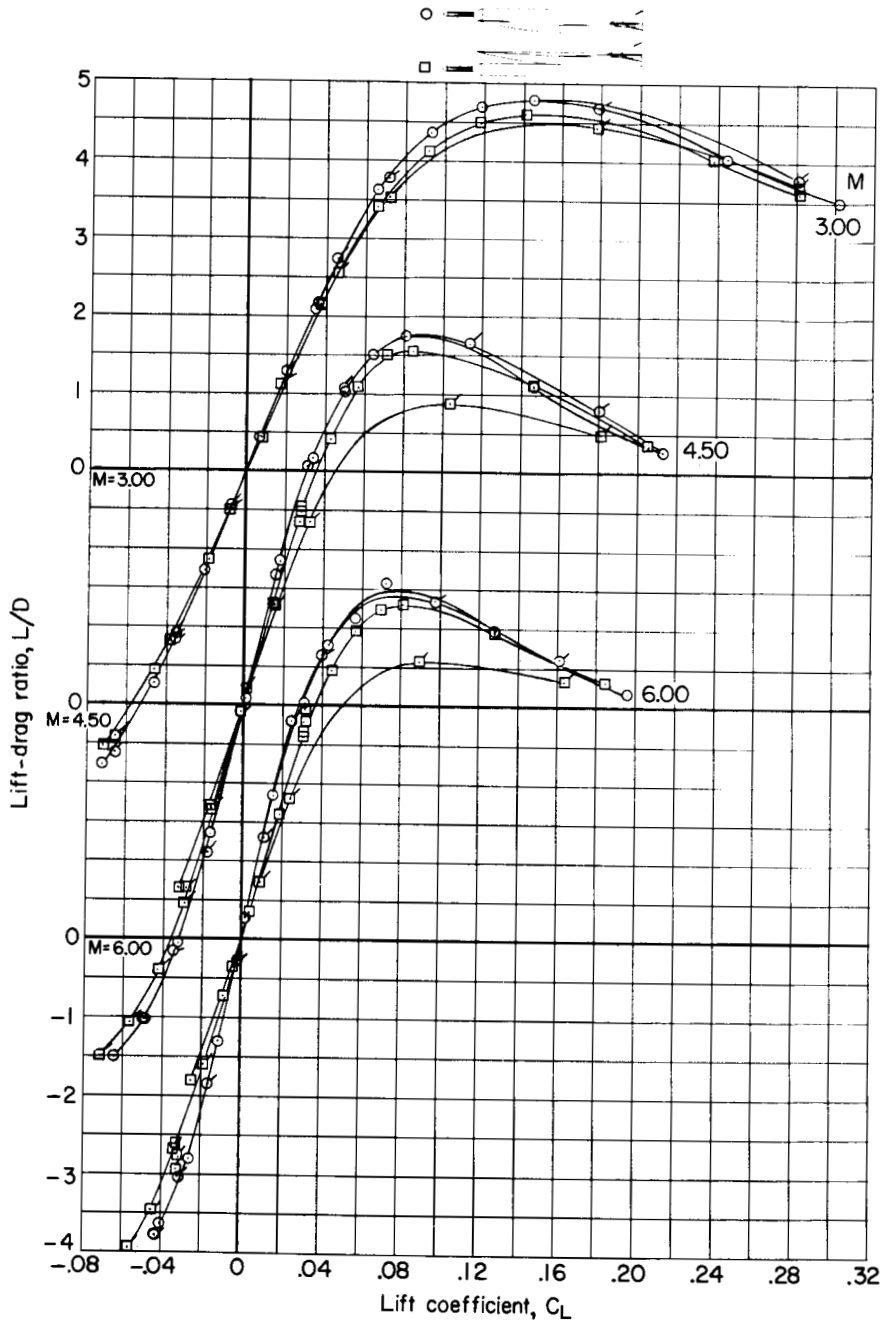

(d) Variation of lift-drag ratio with lift coefficient.

Figure 6.- Concluded.

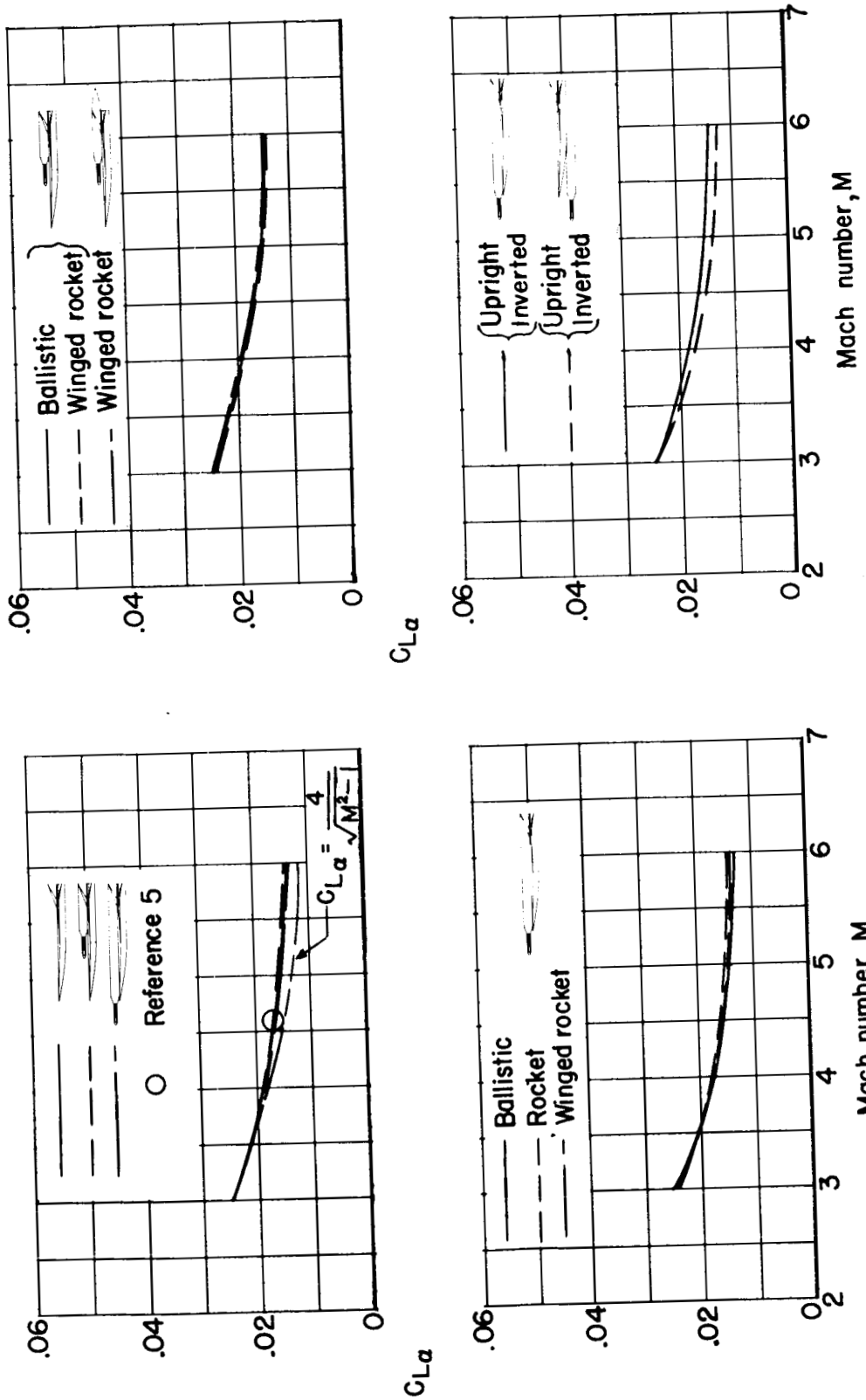

Figure 7.- Variation with Mach number of lift-curve slope of various test configurations. $\beta = 0^\circ$.

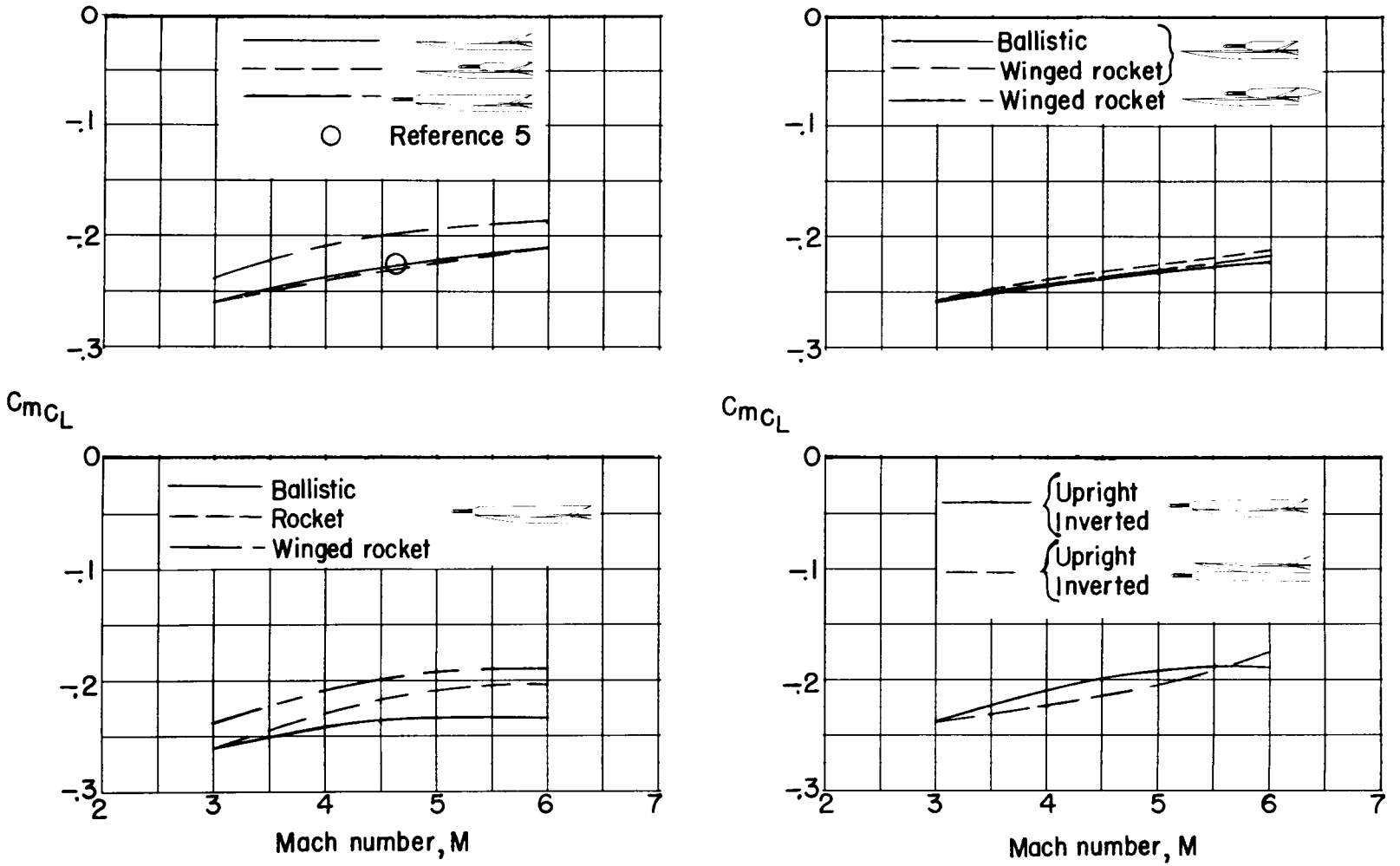

Figure 8.- Variation with Mach number of longitudinal-stability parameters for various test configurations. $\beta = 0^{\circ}$.

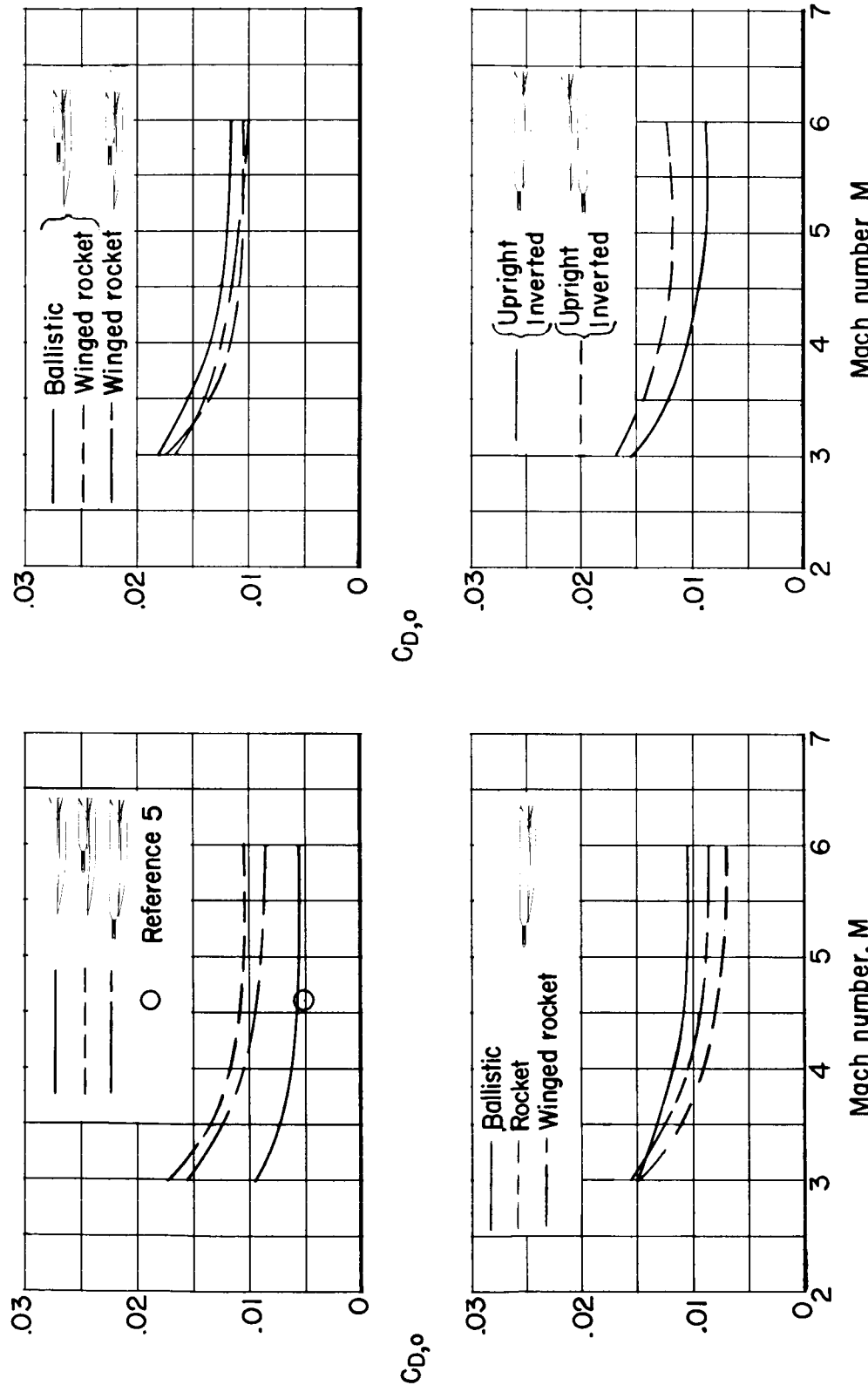

Figure 9.- Variation with Mach number of drag coefficients at zero lift for various test configurations. $\beta = 0^{o}$.

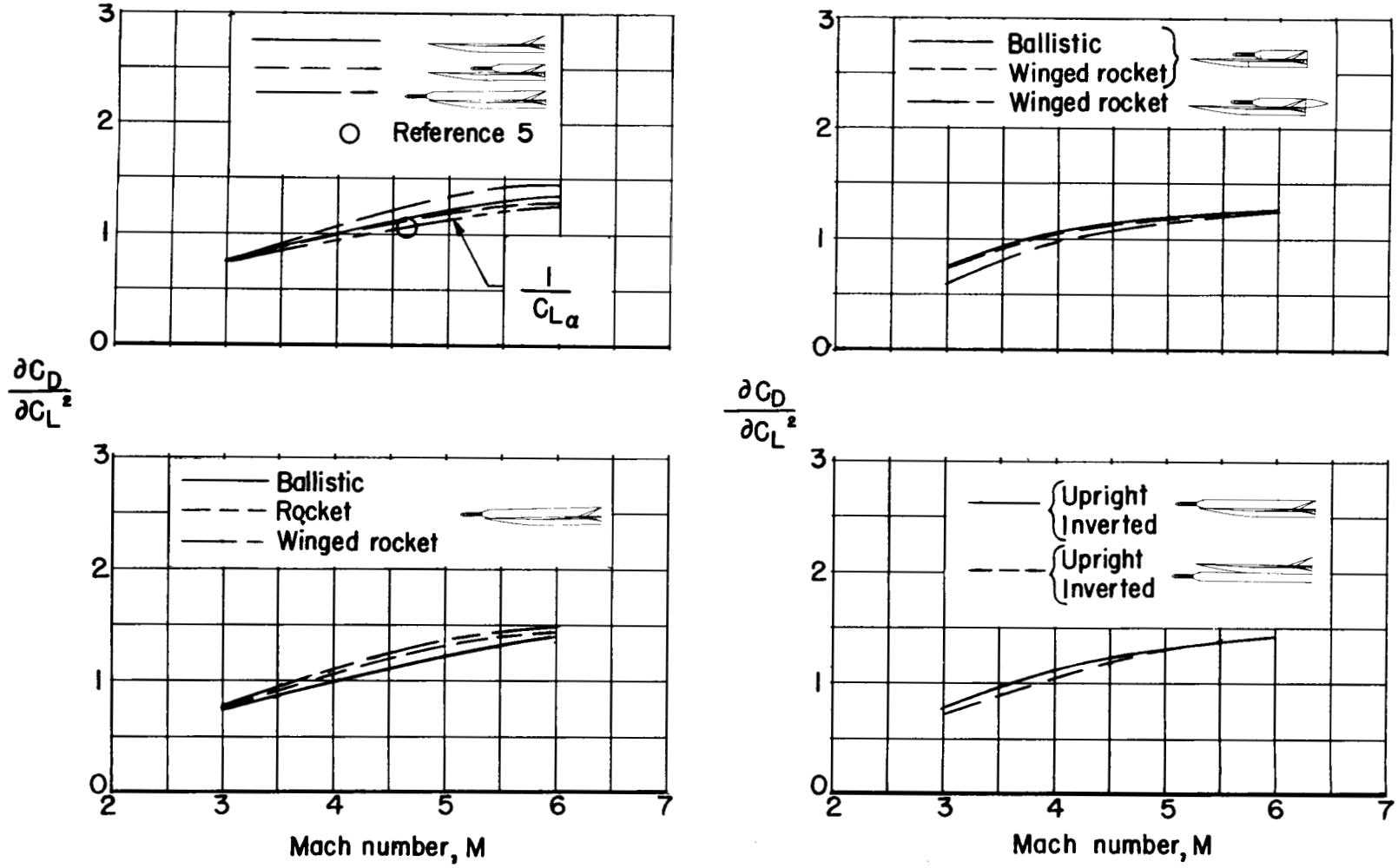

Figure 10.- Variation with Mach number of drag-due-to-lift parameters for various test configurations. $\beta = 0^\circ$.

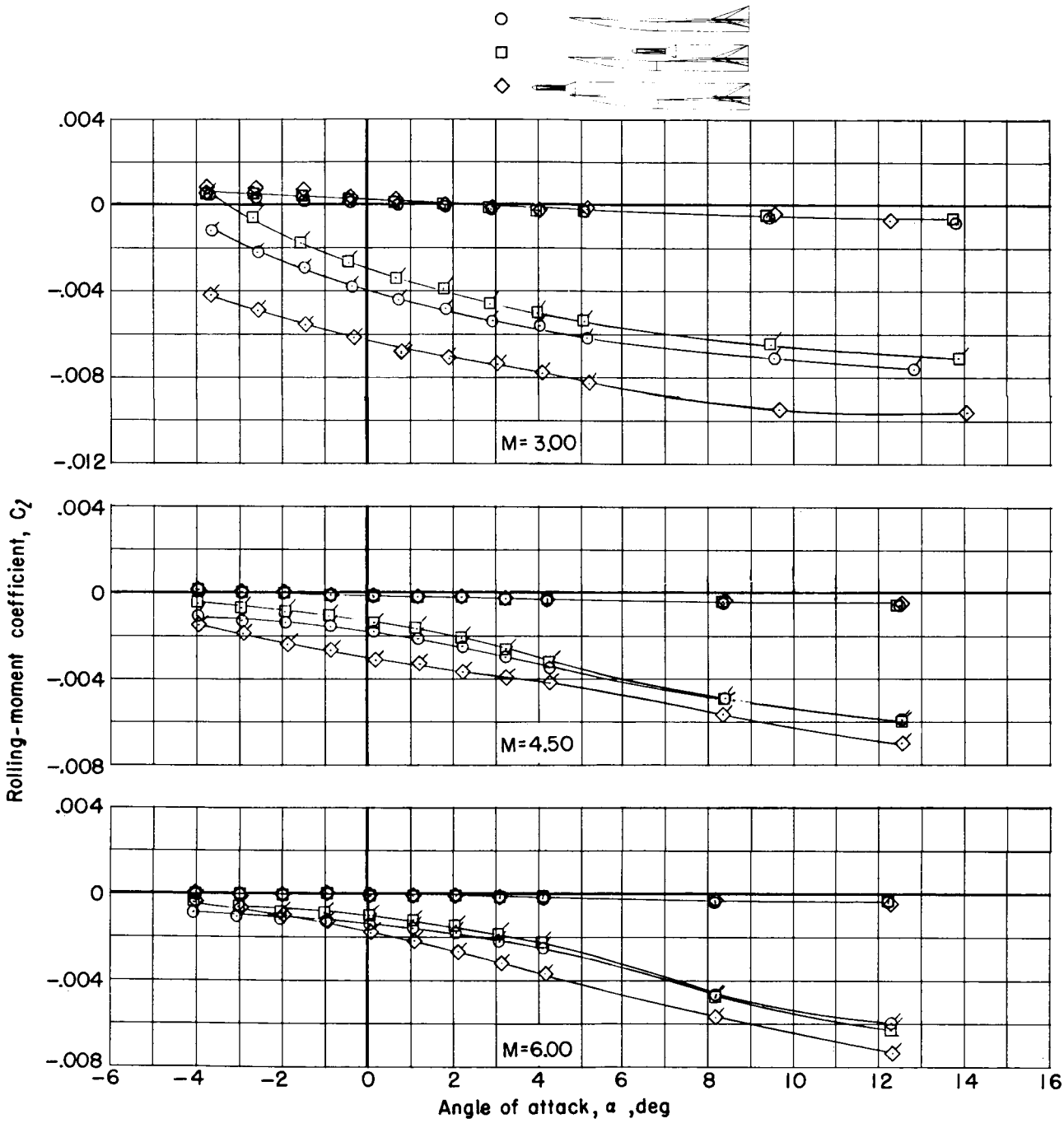

(a) Variation of rolling-moment coefficient with angle of attack.

Figure 11.- Lateral aerodynamic characteristics of first-stage reusable booster compared with launch configurations for short and long second-stage boosters with winged-rocket spacecraft. $\beta = 0^{\circ}$ and 5°. (Flagged symbols refer to $\beta = 5^{\circ}$.)

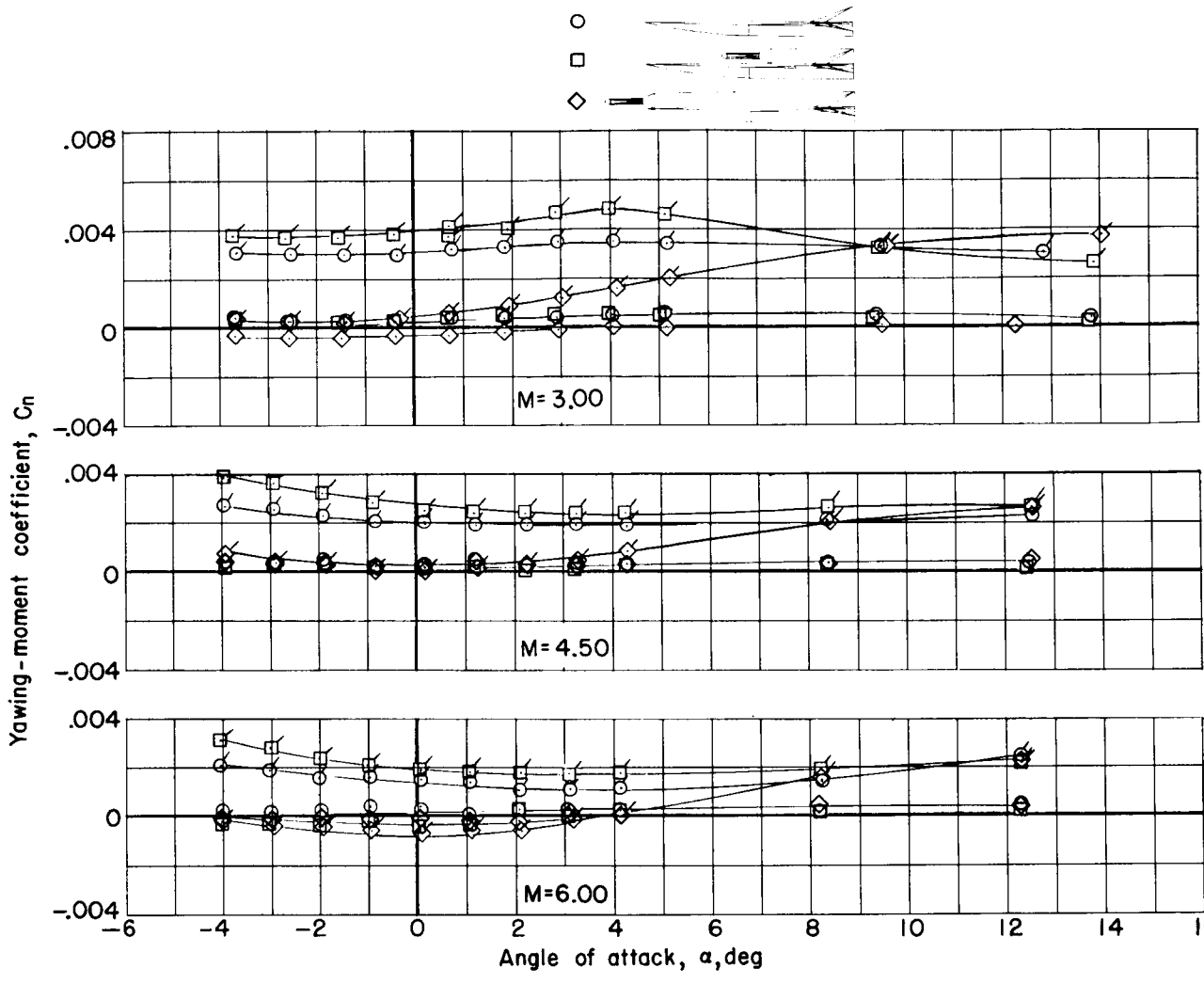

(b) Variation of yawing-moment coefficient with angle of attack.

Figure 11.- Continued.

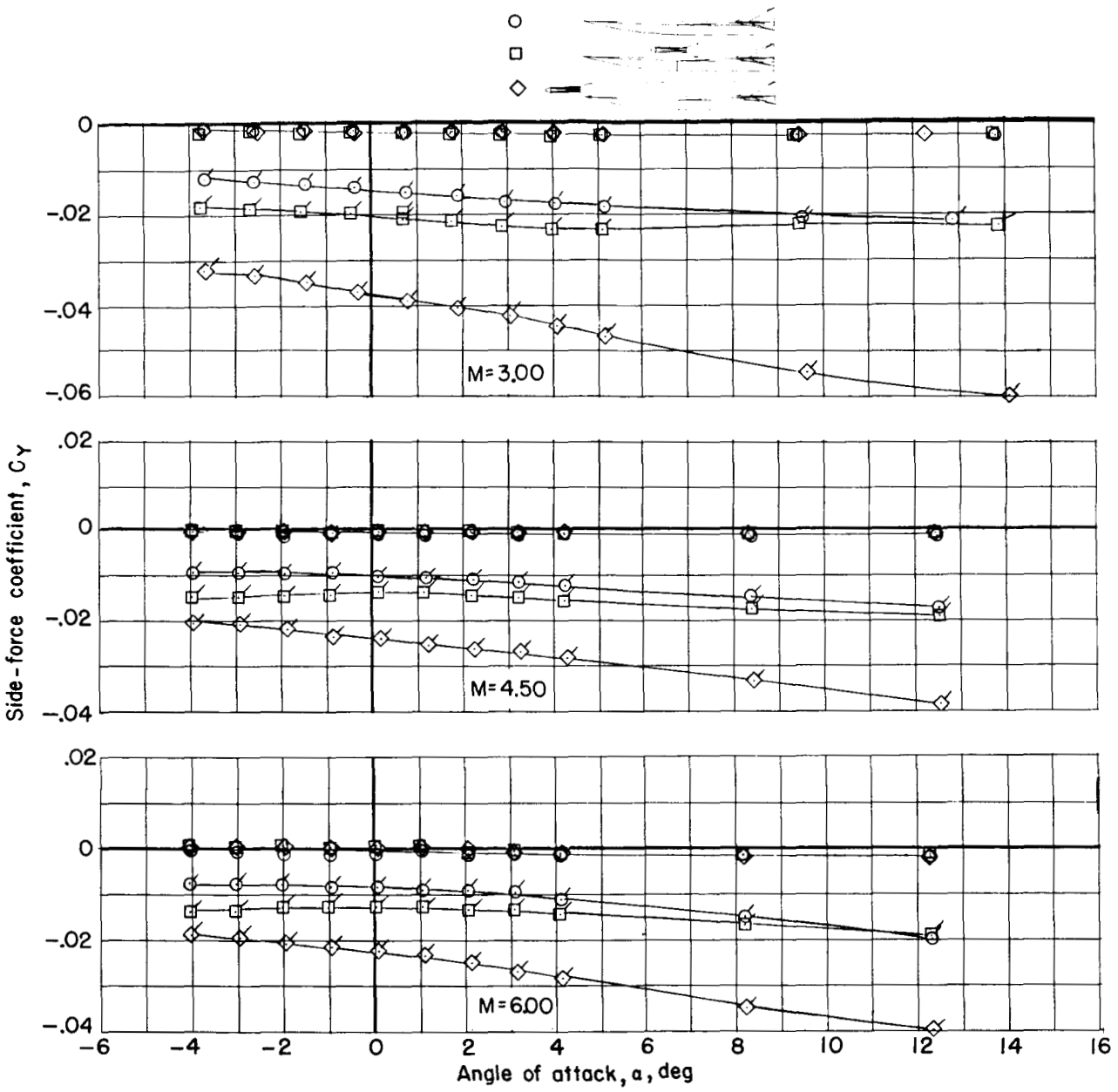

(c) Variation of side-force coefficient with angle of attack.

Figure 11.- Concluded.

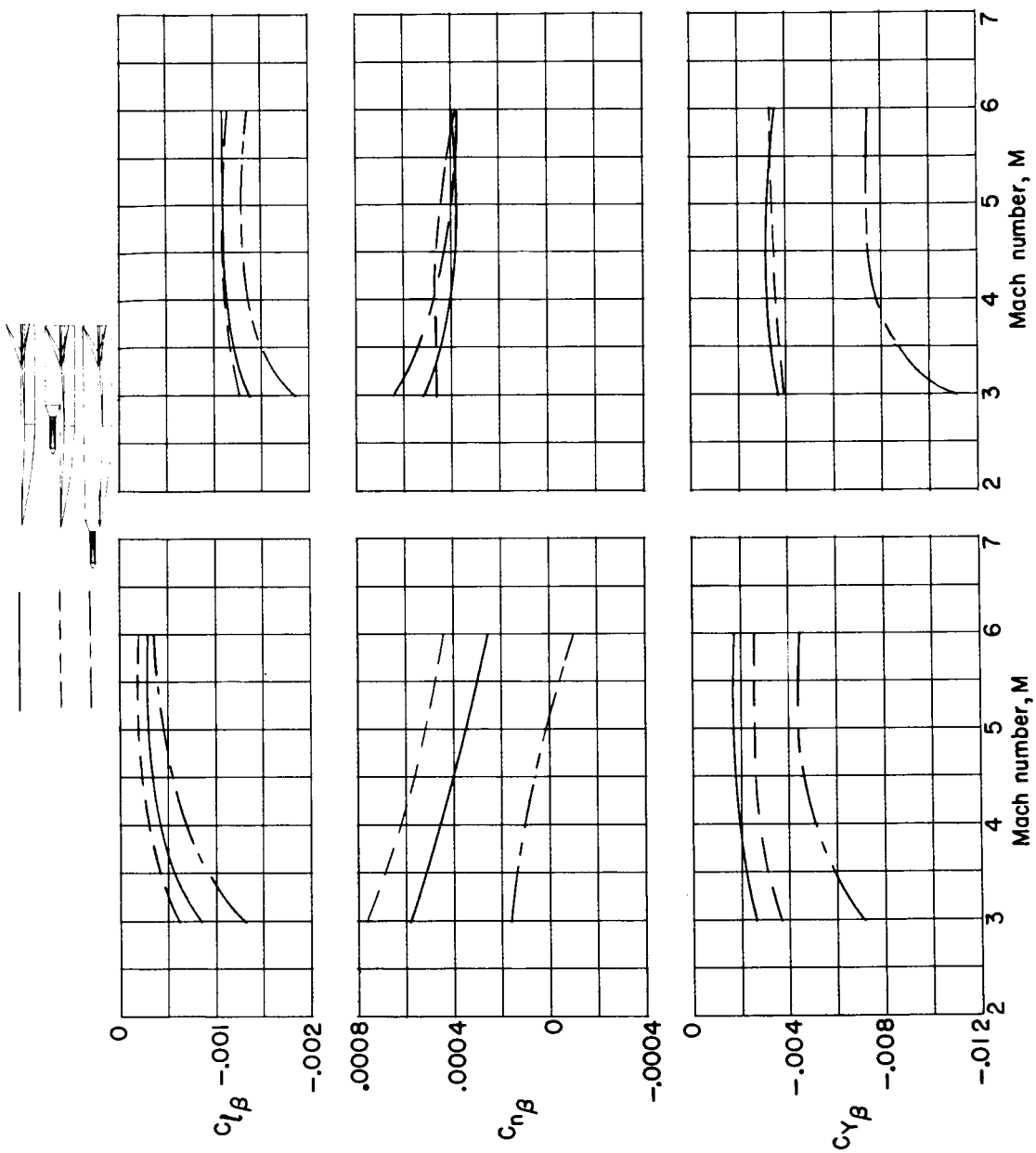

(a) $\alpha = 0^\circ$.

(b) $\alpha = 12^\circ$.

Figure 12.- Lateral-directional stability parameters of first-stage reusable booster compared with launch configurations for short and long second-stage boosters with winged-rocket spacecraft.